Hilbert transform-based semi-analytic meta-model for maximum response envelopes in dynamics of railway bridges

Enrique García-Macías[a], A. E. Martínez-Castro[b]

[a] *Department of Civil and Environmental Engineering, Imperial College London, London SW7 2AZ, UK*
[b] *E.T.S. Ingenieros de Caminos, Canales y Puertos, Av. Fuentenueva sn 18002. Granada, Spain*

Abstract

This paper presents an innovative meta-model for fast assessment of dynamic design envelopes of railway bridges. The proposed approach allows the computation of instantaneous amplitudes of dynamic response time series through the integral Hilbert transform (HT). Based upon the semi-analytic solution of the moving load problem of linear bridge structures, which is analytical in the time domain, the HT is obtained in the Cauchy principal value sense in closed-form. Therefore, the proposed HT-based semi-analytic (HTSA) solution provides a direct estimation of the instantaneous response envelopes of railway bridges under high-speed trains. Since the HT demodulates the signals by suppressing the fast-varying oscillating components, the sampling rates needed for tracing the instantaneous amplitudes are considerably lower than those required for sampling the original signals. Thus, the reduction in computational time achieved by the HTSA approach stems from the sub-sampled approximation of instantaneous envelopes. In order to appraise the effectiveness of the proposed HTSA meta-model, four validation case studies are presented, including mono-dimensional and realistic three-dimensional bridge structures. The presented results report substantial reduction in computational cost with limited accuracy loss, and demonstrate the usefulness of the HTSA meta-model for fast comparison of bridge design alternatives during early design stages.

Keywords: Bridge dynamics, Hilbert transform, Meta-model, Moving loads, Semi-analytic solution, Train-induced vibrations

1. Introduction

Transport policies of the European Union (EU) are geared towards inter-modal Mobility-as-a-Service (MaaS) solutions for passengers and freight, as well as slashing CO_2 emissions and tackling climate change. The latest Commission 2011 Transport White Paper [1] aims to shift 30% of road freight to railway or water-borne transport by 2030, and 50% by 2050. In this context, high-speed railways (HSRs) play a strategic role, since these constitute the terrestrial transport mean with the lowest greenhouse gas emissions and offer vast reductions of transport externalities [2]. Specifically, the White Paper envisions that the length of the high-speed lines will be tripled by 2030, and important investments have been allocated to the construction of high-speed rail corridors in the frame of the Trans-European Transport Networks (TEN-T) to interconnect EU's member states. From an engineering perspective, the design of high-speed rail infrastructure is a complex endeavour due to the extremely high dynamic loads transmitted by passing trains. This is particularly challenging in the design of railway bridges, where resonance and dynamic amplification phenomena hamper the compliance with ultimate and serviceability limit states [3, 4]. Specifically, most design standards such as the Eurocode [5] or the UIC [6] limit the maximum vertical deck accelerations to prevent track instabilities and ensure the comfort of passengers. These constitute severe constraints in the design of rail bridges and must be considered during early concept design stages [7]. Nonetheless, most current dynamic analysis procedures require large computational burdens, which poses a major limitation in the comparison of design alternatives and structural optimization.

In order to comply with the goals stated by the European Commission White Paper, in-depth research efforts must be made, including (i) the seek for efficient methods that allow assessing which share of the existing infrastructure can be upgraded to future high-speed demands with sufficient safety margins; (ii) computationally efficient approaches for the design of new railway infrastructure; and (iii) optimal solutions accounting for resilience, life-cycle cost and return on investments. In general, dynamic effects are often included by means of increasing the static response by Dynamic Amplification Factors (DAFs). Expressions for determining DAFs for real train loadings are provided by design codes such as the Eurocode (see Eurocode annex C [5]), although several

Email address: e.garcia-macias@imperial.ac.uk (Enrique García-Macías)

research works in the literature have reported that these may be over-conservative. For instance, it is worth noting the work by Goicolea *et al.* [8] who demonstrated that the DAFs given by the Eurocode overestimate the dynamic amplification of railway bridges for certain train speeds and axle distances. In addition, current design codes also prescribe limit states for maximum vertical deck accelerations, which are usually decisive in the design of railway bridges. Such criteria address serviceability and safety needs related to track alignment and stability issues, and arose as a result of the ballast instability phenomena found for the first time in the Paris-Lyon HSL [9]. Ensuing investigations ascribed this phenomenon to vertical deck accelerations of the order of 0.7-0.8 g within the critical frequency range of 0-30 Hz [9, 10].

The estimation of maximum deck accelerations of railway bridges requires the solution of the associate moving-load-induced-vibration problem. This problem has drawn the attention of researchers during the last decades, and diverse approaches have been proposed in the literature, most of them included in the review work by Ouyang [11]. These comprise from simplified single-degree-of-freedom (SDOF) techniques to more sophisticated approaches including vehicle-bridge and/or soil-bridge interactions [12–16]. For a comprehensive survey on the application of these approaches to railway bridges, readers may refer to the book of Frỳba [17]. Recent research works, such as the one presented by Cantero and co-authors [18], report that train-track-bridge (TTB) interactions may alter the modal features of light flexible bridges and, as a result, the moving loads problem is eminently non-linear. Step-by-step numerical integration approaches, such as the popular Newmark-β method, become imperative in these cases to solve the coupled non-linear vibration problem. Conversely, less time-intensive modal superposition approaches are well-suited for bridges with masses largely exceeding the train weights, such as concrete and steel bridges with ballasted or slab tracks [19]. In these cases, trains can be simply modelled as massless tandem loads moving at constant speeds. While modal superposition approaches are considerably less computationally demanding, their solution usually requires the use of step-by-step numerical integration methods, and only some analytical solutions for simplified bridge configurations are available in the literature (see e.g. [20]). As an alternative, Martínez-Castro *et al.* [21] proposed a semi-analytic solution for the dynamic analysis of railway bridges under massless moving loads. The strength of that solution lies in the fact that, while the spatial domain is approached by the finite element method (FEM) and modal superposition, the solution is analytical in the time domain. Unlike step-by-step schemes, the sampling frequency in the semi-analytic solution only depends on resolution requirements for maxima detection, since the solution is analytical in the time domain and no numerical integration errors are present. In this framework, the authors recently proposed a meta-model for fast assessment of the maximum response of railway bridges based on the train speed sensitivity (TSS) of the dynamic response envelope curves [22]. Leveraging the closed-form definition of the semi-analytic solution in the time domain, the TSS of the envelope curves was also obtained in closed-form. In this way, the TSS meta-model obtains the design envelopes by moderately sampling the design range of train speeds, while the values at non-sampled speeds are computed using a TSS-based cubic interpolation. The reported results showed large reductions in computational times ($\approx$ 80%), demonstrating its effectiveness for comparison of design alternatives during pre-design stages of railway bridges. In line with our previous work in [22], this paper presents an innovative meta-model based upon the HT of the semi-analytic solution.

The Hilbert transform is a linear time-invariant filter used in signal processing and in the analysis of non-linear and non-stationary signals with manifold applications [23], including mechanical system identification, communication systems, geophysics, seismology, fluid mechanics, medical imaging, etc. Unlike other integral transforms, such as Fourier or Laplace, the HT is not a transform between different domains [24]. Instead, it assigns a complementary imaginary signal to a real one (or vice versa) forming a so-called analytical signal, useful for assessing instantaneous signal attributes such as amplitude (envelope) and frequency [25]. In the realm of Structural Engineering, most efforts have been devoted to the application of the HT to modal system identification and damage detection. The pioneering works of Simon and Tomlinson [26] and Tomlinson [27] investigated the use of the HT to identify deviations of frequency response functions (FRFs) as damage indicators. A noteworthy contribution was made by Feldman [28–30] who proposed the application of the HT to extract time-varying modal features of structures, and showed that it is possible to identify backbone curves from experimental data. While effective for studying quasi-harmonic signals, experimental results such as those reported by Brancaleoni *et al*. [31] on damage detection of bridge structures evidenced that multicomponent signals do not admit well-behaved HTs. As a solution, Huang *et al*. [32–34] proposed in 1998 a revolutionary method named Hilbert-Huang transform (HHT) for the analysis of multi-component signals. The original contribution of the HHT is known as the Empirical Mode Decomposition (EMD). This consists of the decomposition of a signal in terms of elemental components, termed intrinsic mode functions (IMFs), which do admit well-defined HTs. The HHT have been successfully applied to system identification and Structural Health Monitoring (SHM) of SDOF and multi-degree-of-freedom (MDOF) systems [35–41], and a thorough state-of-the-art review can be found in reference [42].

Given that the determination of maximum response envelopes is the cornerstone in the design of railway bridges, the application interest of the HT appears evident. Nevertheless, HTs are typically obtained by signal

convolution with the Hilbert kernel $(\pi t)^{-1}$, with t being the time variable, as shown later in the paper. This requires the signals to be known beforehand, thereby its application for fast assessment of maximum bridge responses is impractical. In this work, an innovative dynamic analysis approach is proposed for the assessment of response envelopes of railway bridges through the HT of the semi-analytic solution proposed by Martínez-Castro *et al.* [21]. To do so, the HT of the semi-analytic solution in the time domain is obtained in the Cauchy principal value sense in closed-form. To the best of the authors' knowledge, the presenting approach is the first solution reported in the literature for the direct estimation of the instantaneous response envelopes of railway bridges under passing trains. Since the Hilbert demodulation suppresses the fast-varying components in the dynamic response, the sampling requirements for detecting global maxima of instantaneous envelopes are considerably lower. This approach constitutes a meta-model for fast assessment of design envelopes and, unlike our previously reported TSS meta-model [22], the reduction of computational times is obtained by decreasing the time frequency sampling. In order to demonstrate the effectiveness of the proposed HTSA solution, four validation case studies are presented. These include two mono-dimensional bridge structures, and two realistic three-dimensional bridges, namely the concrete viaduct of Rodenillo and the bowstring-arch composite steel-concrete viaduct of Santa Ana in Spain. The reported results show substantial decreases in computational times, and demonstrate the capability of the HTSA approach for conducting fast comparisons of bridge design alternatives.

The remaining of the paper is organized as follows: Section 2 introduces the concept of the HTSA approach. Section 3 concisely overviews the theoretical fundamentals of the semi-analytic solution. Section 4 outlines the fundamentals of the HT, and presents the theoretical framework of the proposed HTSA approach. Section 5 reports the validation case studies and discussion and, finally, Section 6 concludes the paper.

2. Concept of the HTSA approach

The dynamic analysis of railway bridges implies high computational costs due to the large number of direct evaluations required for the assessment of maximum response envelopes. Specifically, a number of time series of the dynamic response of the bridge structure (in terms of e.g. vertical deck accelerations, displacements, end rotations, or deck twists) must be computed under the passage of trains at discrete speeds covering the range of design speed. For instance, let us hypothesize a design speed range of 20-420 km/h and a train speed-step Δv = 1 km/h. Considering the ten trains comprised in the HSLM-A (High Speed Load Model) and three ballast mass density assumptions from Eurocode 1 [5], the number of time series to be evaluated amounts to 12030. The computational burden involved in such a large number of evaluations may be prohibitive for 3D bridges with an elevated number of degrees of freedom (DOFs), large number of vibration modes (with resonant frequencies up to 30 Hz [5]), and/or low damping values. Figure 1 shows an example of an acceleration time series computed in the viaduct of Rodenillo (later introduced in Section 5) under the passage of the AVE train at 350 km/h. This has been obtained using the semi-analytic solution in [21] with a sampling frequency of 300 Hz, which leads to 3637 data point evaluations. From this analysis, only the maximum acceleration value a_{max} = 0.35 m/s^2 is retrieved to build the design envelope. Therefore, while the amount of data generated in the dynamic analysis of railway bridges is extensive, only a small fraction is used for the construction of design envelopes.

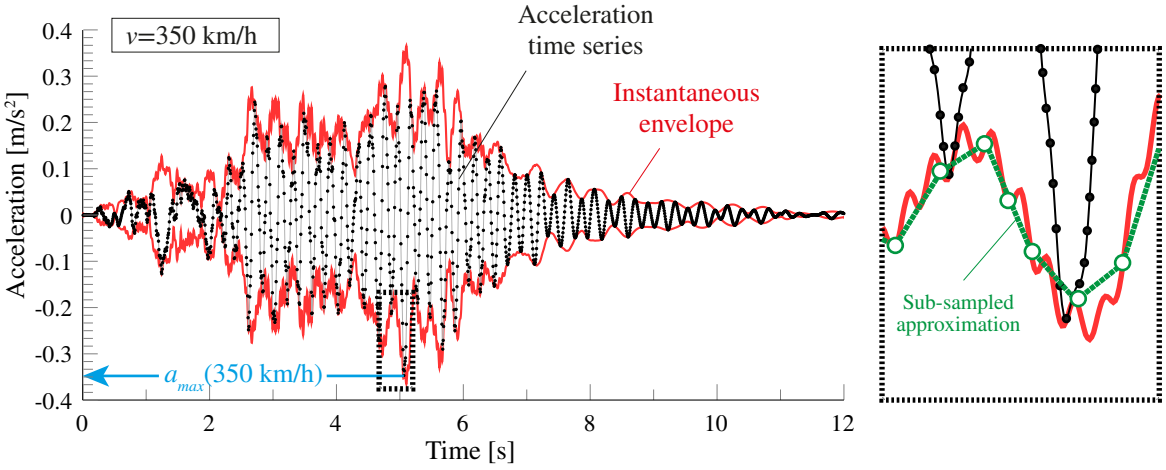

Figure 1: Concept of the proposed HTSA approach. Acceleration time series at the centre of the deck at mid-span of the third span of the viaduct of Rodenillo under the passage of the AVE train at 350 km/h.

The previous discussion motivates the development of meta-models based upon the detection of global maxima of response time series. In particular, the presenting HTSA approach proposes the assessment of the instantaneous envelope of the response time series of railway bridges using the HT. As shown in the example of Fig. 1, the instantaneous envelope of the signal minimizes its fast-varying component. Alternatively, the sensitivity of the envelope to the sampling frequency, that is to say the error caused by sub-sampling, is considerably smaller than that of the original signal. Therefore, it is possible to obtain fast evaluations of the global maxima by using a sub-sampled instantaneous envelope, without incurring large accuracy losses.

3. The semi-analytic solution

Before the introduction of the proposed HTSA approach, a concise overview of the basic semi-analytic solution is presented herein. For further details, readers can refer to references [21, 22, 43, 44]. The semi-analytic solution consists of two consecutive steps: (i) linear modal analysis of the bridge structure using a numerical model, such as an FEM model; and (ii) analytical solution of the bridge response in the time domain under moving loads.

Since the bridge structure is assumed to behave linearly, its response to general train loads can be obtained by linear superposition of the fundamental solution for one single moving load. Assuming one single point load P crossing the bridge at a constant speed v, one can write the resulting time-dependent load as $p(x,t) = P\delta(x - vt)$, with δ being the Dirac delta function, and x and t denoting the longitudinal coordinate along the load lane and the time variable, respectively. Let us define a finite element $e \equiv \left\{x : x \in \left[x_i^e, x_j^e\right]\right\}$ of length $l^e = x_j^e - x_i^e$ lying along the load lane, with x_i^e and x_j^e being the spatial x-coordinates of its initial and terminal points, respectively. Also, let x^e be the abscissa relative to the origin of the element, i.e. $x^e = x - x_i^e$. On this basis, the vertical displacement $w^e(x,y,z,t)$ of an arbitrary point (x,y,z) in the element e can be obtained by modal expansion as:

$$w^e(x,y,z,t) = \sum_{n=1}^{m} q_n(t)\,\phi_n^e(x,y,z), \tag{1}$$

where the term $q_n(t)$ denotes the n-th time-dependent modal amplitude or generalized coordinate, and $\phi_n^e(x,y,z)$ is the n-th mode shape evaluated at (x,y,z). The number m of vibration modes to be accounted for in the dynamic analysis is generally prescribed by design codes (e.g. Eurocode 1 [5] sets this limit to all the vibration modes with resonant frequencies up to 30 Hz). Additionally, the semi-analytic solution assumes that the discretization of the bridge structure enables the consideration of equivalent 1D beam-type DOFs along the load lane. In other words, it is hypothesized that the displacement field of an arbitrary point in the lane can be extrapolated from the displacements, w, and slopes, $\theta_x = \partial w/\partial x$, at the discretized nodes. In this wise, the displacement field along the load lane can be characterised by Hermite cubic spline shape functions, $h_i(x^e)$, in such a way that Eq. (1) can be rewritten with no explicit dependence on variables y and z as:

$$w^e\left(x^e,t\right) = \sum_{n=1}^{m} q_n(t) \sum_{i=1}^{4} G_{ni}^e\, h_i\left(x^e\right), \tag{2}$$

where the matrix coefficients G_{ni}^e represent the evaluation of the mode shapes along the load lane. Functions $q_n(t)$ in Eq. (2) were obtained by Martínez-Castro *et al.* [21] in closed-form as the sum of a homogeneous and a particular solution, $q_n(t) = q_n^h(t) + q_n^p(t)$, given by:

$$q_n^h\left(\tau\right) = e^{-\zeta_n\omega_n\tau}\left[A_n\cos\left(\omega_n^d\tau\right) + B_n\sin\left(\omega_n^d\tau\right)\right], \tag{3}$$

$$q_n^p\left(\tau\right) = \alpha_n^{(0)} + \alpha_n^{(1)}(v\tau) + \alpha_n^{(2)}(v\tau)^2 + \alpha_n^{(3)}(v\tau)^3, \tag{4}$$

with $\tau = t - x_i^e/v$ being the local time for element e, and A_n and B_n coefficients of the homogeneous solution. Terms ω_n and $\omega_n^d = \omega_n\sqrt{1-\zeta_n^2}$ in Eq. (3) stand for the undamped and damped natural angular frequencies of the *n-th* mode, with ζ_n being its modal damping ratio. Coefficients $\alpha_n^{(i)}$ in Eq. (4) are defined as:

$$\begin{aligned}
\alpha_n^{(0)} &= v^3\alpha_n^{(01)} + v^2\alpha_n^{(02)} + v\alpha_n^{(03)} + \alpha_n^{(04)},\\
\alpha_n^{(1)} &= v^2\alpha_n^{(11)} + v\alpha_n^{(12)} + \alpha_n^{(13)},\\
\alpha_n^{(2)} &= v\alpha_n^{(21)} + \alpha_n^{(22)},\\
\alpha_n^{(3)} &= \alpha_n^{(31)},
\end{aligned} \tag{5}$$

with coefficients $\alpha_n^{(ij)}$ given in [21] as functions of the modal properties (i.e. mode shapes, natural frequencies and damping ratios) and the length of the load lane segment. Furthermore, coefficients A_n and B_n in Eq. (3) are obtained from the initial conditions $q_n^0 = q_n(0)$ and $\dot{q}_n^0 = \dot{q}_n(0)$, with overdots denoting time derivative, as follows:

$$A_n = q_n^0 - \alpha_n^0, \tag{6}$$

$$B_n = \frac{\dot{q}_n^0 + \zeta_n \omega_n A_n - \alpha_n^{(1)} v}{\omega_n^d}. \tag{7}$$

The complete solution is constructed in a piecewise form by concatenating the solution in Eq. (2) between consecutive elements. At-rest initial conditions are commonly imposed in the first element, that is $q_n(0)|^{e=1} = 0$ and $\dot{q}_n(0)|^{e=1} = 0$. For the remaining elements, C1 inter-elemental continuity is applied as $q_n(0)|^{e+1} = q_n(l^e/v)|^e$ and $\dot{q}_n(0)|^{e+1} = \dot{q}_n(l^e/v)|^e$.

Finally, velocities and accelerations can be readily obtained by time differentiation of $w^e(x, y, z, t)$ in Eq. (1) as:

$$\dot{w}^e(x, y, z, t) = \sum_{n=1}^{m} \dot{q}_n(t) \phi_n^e(x, y, z), \tag{8}$$

$$\ddot{w}^e(x, y, z, t) = \sum_{n=1}^{m} \ddot{q}_n(t) \phi_n^e(x, y, z). \tag{9}$$

4. Theoretical framework of the HTSA approach

4.1. Fundamentals of Hilbert transform

The HT of a function $x(t) \in L^p(\mathbb{R})$, $1 \leq p < \infty$, is a real-valued function $\tilde{x}(t)$ defined by the following integral transform [45–47]:

$$\mathcal{H}[x(t)] = \tilde{x}(t) = \frac{1}{\pi} \mathrm{PV} \int_{-\infty}^{+\infty} \frac{x(s)}{t - s} \mathrm{d}s, \tag{10}$$

where PV stands for the Cauchy principal value of the integral because of a possible singularity at $t = s$, s being the variable of integration. The HT in Eq. (10) can be thought of as the convolution product of $x(t)$ and $(\pi t)^{-1}$, i.e. $\tilde{x}(t) = x(t) * (\pi t)^{-1}$. This is equivalent to a linear filter with transfer function $H(\omega) = -\mathrm{i}\,\mathrm{sgn}(\omega)$, where i denotes the imaginary unit. Therefore, the HT keeps the amplitudes of the spectral components unchanged, but shifts their phases by $-\pi/2$.

The major interest of the HT lies in its capability to extend real-valued functions into analytic signals. An analytic signal, or quadrature projection, is defined as a complex signal whose imaginary part is the HT of the real part, that is [48]:

$$X(t) = x(t) + \mathrm{i}\tilde{x}(t). \tag{11}$$

Analytic signals are typically represented in the form of a phasor rotating in the complex plane as sketched in Fig. 2. A phasor is a vector at the origin of the complex plane of module $A(t)$ and angular position $\psi(t)$. On this basis, an analytic signal can be expressed in terms of its time-variant magnitude and phase angle in trigonometric or exponential form as [25]:

$$X(t) = A(t)\left[\cos\psi(t) + \mathrm{i}\sin\psi(t)\right] = A(t)\, e^{\mathrm{i}\psi(t)}, \tag{12}$$

and its instantaneous amplitude and phase read:

$$A(t) = \pm|X(t)| = \pm\sqrt{x^2(t) + \tilde{x}^2(t)}, \quad \psi(t) = \arctan\frac{\tilde{x}(t)}{x(t)}. \tag{13}$$

Geometrically, the envelope means an integral curve which determines a singular position of the initial function. The form or the shape of the variation of the instantaneous amplitude is called a wave envelope. An initial signal and its envelope have common tangents at points of contact, and the signal never crosses the envelope. By using the HT, the rapid oscillations can be removed from the amplitude modulated signal to produce a direct representation of the slow envelope alone.

For a comprehensive survey of the mathematical properties of the HT, readers are referred to [30, 46, 47]. Nevertheless, owing to its importance in the subsequent theoretical derivations, it is worth outlining herein the

product theorem or Bedrosian identity. Let $x(t)$ and $y(t)$ be two real-valued signals with non-overlapping spectra, i.e. their Fourier transforms satisfy the conditions, $X(\omega) = 0$ for $|\omega| \geq \omega_c$, and $Y(\omega) = 0$ for $|\omega| < \omega_c$, where ω_c is a certain cut-off frequency. Under these conditions, the Bedrosian identity states that the HT of the product of the signals can be obtained as [49]:

$$\mathcal{H}\left[x(t)y(t)\right] = x(t)\mathcal{H}\left[y(t)\right]. \tag{14}$$

In virtue of this identity, the HT of an amplitude-modulated signal can be obtained by transforming only the high-pass component. This is, for instance, the case of exponentially decaying vibrations, where a fast oscillating signal is modulated by a slowly varying exponential decay term.

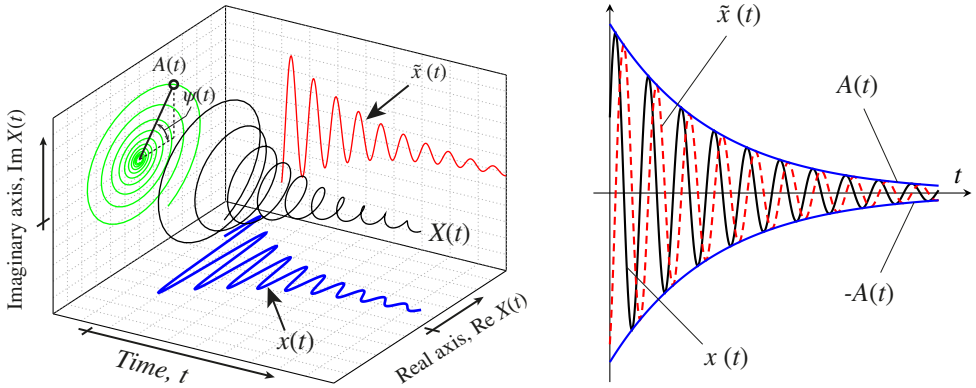

Figure 2: Geometrical representation of an analytic signal $X(t)$, real signal $x(t)$, HT $\tilde{x}(t)$, module $A(t)$ and angular position $\psi(t)$ of the phasor representation.

4.2. Hilbert transform of the semi-analytic solution

The HT of the semi-analytic solution previously outlined in Section 3 is obtained by the integral operator in Eq. (10) at every time step t throughout the complete time domain. This includes both the solution for forced and free vibrations, so the HT of the semi-analytic solution can be written on the basis of the homogeneous and particular solutions in Eqs. (3) and (4) as:

$$\tilde{q}(t) = \frac{1}{\pi}\,\mathrm{PV}\int_{-\infty}^{+\infty}\frac{q(s)}{t-s}\mathrm{d}s = \frac{1}{\pi}\left\{\sum_{e=1}^{N}\mathrm{PV}\int_{0}^{l^e/v}\frac{q^h(s)+q^p(s)}{\tau-s}\mathrm{d}s\right\} + \frac{1}{\pi}\left\{\mathrm{PV}\int_{0}^{+\infty}\frac{q^h(s)}{\tau-s}\mathrm{d}s\right\}, \tag{15}$$

where subscripts n have been omitted for notational convenience. Note that the first term in the right hand side relates the Hilbert integral throughout the load lane elements of the bridge ($e \in [1, N]$), while the second term accounts for the free vibration solution once the load has left the structure. Given that the HT is essentially a linear operator, the HT in Eq. (15) can be constructed from the transform of the homogeneous and particular solutions separately. Let us first focus on the homogeneous solution given in Eq. (3). It is straightforward to recognize that the exponential term represents a low-pass or slow-varying component ($q^h_{slow}(\tau)$), while the sinusoidal terms provide the oscillating or high-pass component of the response ($q^h_{fast}(\tau)$). Therefore, in light of the Bedrosian identity previously introduced in Eq. (14), the HT of the homogeneous solution can be simplified as follows:

$$\tilde{q}^h(\tau) = q^h_{slow}(\tau)\,\tilde{q}^h_{fast}(\tau) = \frac{1}{\pi}\,e^{-\zeta_n\omega_n|\tau|}\,\mathrm{PV}\int_{0}^{l^e/v}\frac{q^h_{fast}(s)}{\tau-s}\mathrm{d}s. \tag{16}$$

Note that relative time τ appears in absolute value in the exponential term in Eq. (16). This imposes a mirroring of this term around $\tau = 0$, and avoids the uncontrolled exponential growth of the solution when $\tau < 0$. In virtue of the closed-form semi-analytic solution in the time domain, the primitive or indefinite integral of the integrand in Eq. (16) can be analytically obtained as $Q^h_{fast}(\tau, s)$:

$$Q^h_{fast}(\tau,s) = \mathrm{Si}\left(\omega_n^d\,(s-\tau)\right)\left[A_n\sin\left(\omega_n^d\tau\right) - B_n\cos\left(\omega_n^d\tau\right)\right] - \mathrm{Ci}\left(\omega_n^d\,(s-\tau)\right)\left[A_n\cos\left(\omega_n^d\tau\right) + B_n\sin\left(\omega_n^d\tau\right)\right], \tag{17}$$

where Si and Ci denote the sine and cosine integral functions given by:

$$\mathrm{Si}(z) = \int_0^z\frac{\sin(s)}{s}\mathrm{d}s, \tag{18}$$

$$\mathrm{Ci}(z) = -\int_0^z \frac{\cos(s)}{s}\mathrm{d}s. \tag{19}$$

On this basis, and given that the semi-analytic solution in Eq. (15) is Hölder continuous (cf. [50]), the HT of the high-pass component of the homogeneous part in Eq. (16) can be obtained in the Cauchy principal value sense as:

$$\tilde{q}^h_{fast}(\tau) = \frac{1}{\pi}\left(\lim_{s\to l_i^e/v-\varepsilon} Q^h_{fast}(\tau, s) - \lim_{s\to\varepsilon} Q^h_{fast}(\tau, s)\right), \tag{20}$$

where ε is a small positive number tending to zero, i.e. $\varepsilon \to 0^+$. A similar treatment can be applied to the particular solution. In this case, the primitive involved in the HT of the particular solution in Eq. (4) can be obtained in closed-form as:

$$Q^p(\tau, s) = -v\left\{\frac{1}{6}(s-t)\left[6\alpha_n^{(1)} + v\left(3\alpha_n^{(2)}(s+3t) + \alpha_n^{(3)}\left(2s^2+5st+11t^2\right)v\right)\right] + t\left[\alpha_n^{(1)} + tv\left(\alpha_n^{(2)} + \alpha_n^{(3)}tv\right)\right]\ln|s-t|\right\}, \tag{21}$$

and the HT of the particular solution reads:

$$\tilde{q}^p(\tau) = \frac{1}{\pi}\left(\lim_{s\to l_i^e/v-\varepsilon} Q^p(\tau, s) - \lim_{s\to\varepsilon} Q^p(\tau, s)\right). \tag{22}$$

Finally, the Cauchy principal value of the second term in the right hand side of Eq. (15), i.e. the free vibration term, can be readily obtained as:

$$\begin{aligned}\frac{1}{\pi}\mathrm{PV}\int_0^{+\infty}\frac{q^h(s)}{\tau-s}\mathrm{d}s &= \frac{1}{\pi}\left(\lim_{s\to+\infty} Q^h(\tau, s) - \lim_{s\to\varepsilon} Q^h(\tau, s)\right)\\ &= e^{-\zeta_n\omega_n|\tau|}\left[A_{N+1}\sin\left(\omega_n^d\tau\right) - B_{N+1}\cos\left(\omega_n^d\tau\right)\right] - \frac{1}{\pi}\lim_{s\to\varepsilon} q^h_{slow}(\tau)Q^h_{fast}(\tau, s).\end{aligned} \tag{23}$$

4.3. Implementation details of the general HTSA approach for complete train compositions

The implementation of the proposed HTSA approach for a complete train composition is summarised in the pseudo-code shown in Fig. 3. At every instant time t, the n_l axles of a complete train can be divided into those that have already crossed the lane, n_o, those upon the bridge, n_i, and those that have not yet entered the structure, n_s ($n_l = n_s + n_i + n_o$). Each k-th axle is characterized by an axle load, P_k, and a distance d_k from the origin of the bridge. On this basis, the semi-analytic solution $q_n(t)$ is expanded as:

$$q_n(t) = q_n|_{in}(t) + q_n|_{out}(t), \tag{24}$$

where subscripts "*in*" and "*out*" relate the corresponding quantity to the axle loads upon the bridge and those that have already left the structure, respectively. Let superscript "e" denote the element of the lane discretization ($e \in [1, N]$) in which a k-th axle load is located at a distance xi^e from its origin at time t. Therefore, the relative time for the k-th load can be defined as $\tau_k = t - \left(d_k + x_i^e\right)/v$. If the k-th load has left the structure, the relative time takes the expression $\tau_k^{N+1} = t - \left(d_k + x_j^N\right)/v$. In this light, the contributions of the axle loads upon the structure and those that have already left it can be written as:

$$q_n|_{in}(t) = \sum_{k=n_o+1}^{n_o+n_i}\left\{e^{-\zeta_n w_n\tau_k}\left[A_n\cos\left(\omega_n^d\tau\right) + B_n\sin\left(\omega_n^d\tau\right)\right] + \alpha_n^{(0)} + \alpha_n^{(1)}(v\tau) + \alpha_n^{(2)}(v\tau)^2 + \alpha_n^{(3)}(v\tau)^3\right\}P_k, \tag{25}$$

$$q_n|_{out}(t) = \sum_{k=1}^{n_o}\left\{e^{-\zeta_n w_n\tau_k^{N+1}}\left[A_{N+1}\cos\left(w_n^d\tau_k^{N+1}\right) + B_{N+1}\sin\left(w_n^d\tau_k^{N+1}\right)\right]\right\}P_k, \tag{26}$$

where coefficients A_{N+1} and B_{N+1} are selected so that the compatibility of the solution is enforced in free vibration once the loads have crossed the bridge. Afterwards, the HT of the semi-analytic solution in Eq. (15) is performed accounting for the contribution of all the axle loads as:

$$\tilde{q}(t) = \sum_{k=1}^{n_l}\frac{1}{\pi}\left\{\sum_{e=1}^{N}\mathrm{PV}\int_0^{l^e/v}\frac{q^h(s)+q^p(s)}{\tau-s}\mathrm{d}s + \mathrm{PV}\int_0^{+\infty}\frac{q^h(s)}{\tau-s}\mathrm{d}s\right\}P_k, \tag{27}$$

The Cauchy principal values involved in the first and second terms in the right hand side of Eq. (27) are obtained by applying the limits previously reported in Eqs. (20) and (23), respectively (ε = 1.0E-15). The evaluation of the sine and cosine integral functions in Eq. (17) can be computationally expensive. In this work, the rational series expansions given by Abramowitz and Stegun [51] for an absolute error less than 5E-7 are used to accelerate their evaluation. Once the semi-analytic solution, $w^e(x^e,t)$, and its HT, $\widetilde{w}^e(x^e,t)$, have been obtained, the analytical signal in Eq. (11) is constructed and its module is computed to obtain the instantaneous envelope $A^e(x^e,t)$ as:

$$A^e(x^e,t) = \sqrt{w^e(x^e,t)^2 + \widetilde{w}^e(x^e,t)^2}. \tag{28}$$

The proposed technique has been implemented in a FORTRAN computer code on a standard desktop PC.

Procedure: **HTSA**

Linear Modal Analysis
Get ϕ_n^e, ω_n, G_{ni}^e
Get $\alpha_n^{(ij)}$
Get $[A_n, B_n]_{e=1}^{N+1}$
Get $\left[\alpha_n^0, \alpha_n^1, \alpha_n^2, \alpha_n^3\right]_{e=1}^{N}$

Set $t = 0$
while $t < T_t$ **do**
  Get n_i, n_o
  Set $q_n(t) = 0$
  Set $w^e(x^e,t) = 0$
  Set $\widetilde{w}^e(x^e,t) = 0$
  for $(n = 1;\ n < m;\ n++)$ **do**
    Semi-analytic solution
    for $(k = n_o + 1;\ k \le n_o + n_i;\ k++)$ **do**
      $q_n(t) = q_n(t) + \left(q_n^h(\tau) + q_n^p(\tau)\right) P_k$
    end
    for $(k = 1;\ k \le n_o;\ k++)$ **do**
      $q_n(t) = q_n(t) + q_n^h(\tau) P_k$
    end
    $w^e(x^e,t) = w^e(x^e,t) + q_n(t)\ \sum_{i=1}^{4} G_{ni}^e h_i(x^e)$
    Hilbert transform
    $\widetilde{q}(t) = 0$
    for $(k = 1;\ k \le n_l;\ k++)$ **do**
      $\widetilde{q}(t) = \widetilde{q}(t) + \left(\widetilde{q}_n^h(\tau) + \widetilde{q}_n^p(\tau)\right) P_k$
    end
    $\widetilde{w}^e(x^e,t) = \widetilde{w}^e(x^e,t) + \widetilde{q}_n(t)\ \sum_{i=1}^{4} G_{ni}^e h_i(x^e)$
  end
  Instantaneous envelope
  $A^e(x^e,t) = \sqrt{w^e(x^e,t)^2 + \widetilde{w}^e(x^e,t)^2}$
  $t = t + \Delta t$
end

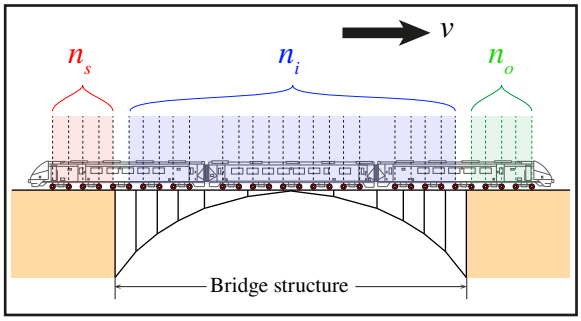

Figure 3: Pseudo-code of the proposed HTSA for maximum response envelopes in dynamics of railway bridges.

4.4. Reduced Hilbert integral transforms: window filtering and infinite extension of highly oscillating terms

Albeit instantaneous envelopes enable the assessment of maximum responses through sub-sampled approximations with limited accuracy losses, the large number of operations involved in the HT poses a major drawback from a computational efficiency standpoint. This is due to the fact that, to compute the HT in Eq. (10), one must know the values of the signal $x(t)$ for all t. In the context of dynamic analysis of railway bridges under train loads, this implies that, at every time step, the Hilbert integral transform must account for all the axles of the train composition throughout all the elements of the load lane, including the range of free vibrations. In order to alleviate the computational burden, a reduced Hilbert integral transform through window filtering is proposed as:

$$\tilde{q}(t) = \frac{1}{\pi}\,\mathrm{PV}\int_{t-d_i/2v}^{t+d_i/2v} \frac{q(s)}{t-s}\mathrm{d}s, \tag{29}$$

with d_i being the window length. This implies that the Hilbert integral transform is only performed in a finite interval of duration d_i/v around the time of evaluation, that is $s \in [t - d_i/2v, t + d_i/2v]$. As a result, the number of load lane elements to be included in the integration decreases, and so does the computational cost. The loss of information on the contribution of the signals outside the window shrinks the demodulation efficiency of the analytic envelope, thereby the window length must be carefully chosen. In particular, the window length must be defined accounting for the distance between axle loads so that the analytical envelope includes the contributive

effect of neighbouring axle loads. Tailored parametric analyses are presented later in Section 5 to scrutinize the effect of the window length on the instantaneous amplitude.

Along with the previous window filtering, an approximation of the HT of the homogeneous solution in Eq. (16) is also proposed based on the infinite extension of highly oscillating terms. This approximation is motivated by the large computational cost involved in the evaluation of the trigonometric integrals in Eq. (17). These arise as a result of applying the Hilbert integral transform throughout the elements of the load lane in Eq. (15), which represent adjoin finite intervals in the time domain. Nevertheless, if the solution exhibits a fast oscillating behaviour within an element, the analytic envelope can be approached considering an infinite extension of the elemental solution. Under this assumption, the HTs of the sinusoidal terms in Eq. (3) approach the fundamental results $\mathcal{H}\left[\cos(t)\right] = \sin(t)$ and $\mathcal{H}\left[\sin(t)\right] = -\cos(t)$. Therefore, the HT of the homogeneous solution in Eq. (3) simply reads:

$$\tilde{q}(t) = e^{-\zeta_n \omega_n \tau}\left[A_n \sin\left(\omega_n^d \tau\right) - B_n \cos\left(\omega_n^d \tau\right)\right]. \tag{30}$$

The correctness of the previous approximation depends upon the frequency content of the signal to be transformed and the discretization of the load lane. Nonetheless, the consideration of modal superposition facilitates the definition of application criteria on the basis of the resonant frequencies of the bridge structure. In particular, sensitivity analyses with moderate load lane discretizations ($l_i^e \approx 2-3$ m) have shown that the application of such an approximation to modal components with resonant frequencies above a cut-off frequency of 10 Hz yields accurate enough results. In this wise, the HT in Eq. (16) can be limited to modal components with frequencies below a certain cut-off frequency, while the computationally inexpensive approximation in Eq. (30) can be assumed for the rest of modal components. The afore-mentioned sensitivity analyses are omitted herein because of space constraints. Nevertheless, interested readers may refer to the supplementary material, where sensitivity analyses of the cut-off frequency are provided for the case study II reported below.

5. Validation case studies and discussion

In this section, four different validation case studies are presented to demonstrate the effectiveness of the proposed approach. In particular, two 1D beam models are presented in Sections 5.1 and 5.2, including a simply supported beam model and a continuous three-span beam model. The first case study allows to appraise the correctness of the HTSA model, since an analytical solution to the moving-load problem is available. Afterwards, the second case study evaluates the influence of the window filtering introduced in Section 4.4. Finally, two realistic 3D bridge models are presented in Sections 5.3 and 5.4. These include a concrete box girder bridge, the viaduct of Rodenillo, and a bowstring-arch composite steel-concrete bridge, the viaduct of Santa Ana. In these case studies, results and discussion focus on the assessment of the effectiveness of the HTSA meta-model in terms of accuracy and computational time. The data used to elaborate all the subsequent results can be found as part of the supplementary material, including commented MATLAB scripts for data processing and plotting.

5.1. Case study I: Simply supported beam.

The first case study is sketched in Fig. 4 (a) and corresponds to a bridge configuration analysed by the Spanish standard for railway bridges IAPF-07 [52]. This consists of a simply supported Euler-Bernoulli beam of length $L = 15$ m, constant mass per unit length $\rho A(x) = 15$ t/m, flexural stiffness $EI(x) = 7694.081$ MPa, and constant modal damping ratio $\zeta = 2\%$. A single point moving load P traverses the bridge at a constant speed v, and it is initially located at a distance d from the origin. Formally, such a load can be written as $p(x,t) = P\delta(x - vt - d)$. The purpose of the definition of distance d is to evaluate the effects of the mirroring previously reported in Eq. (16).

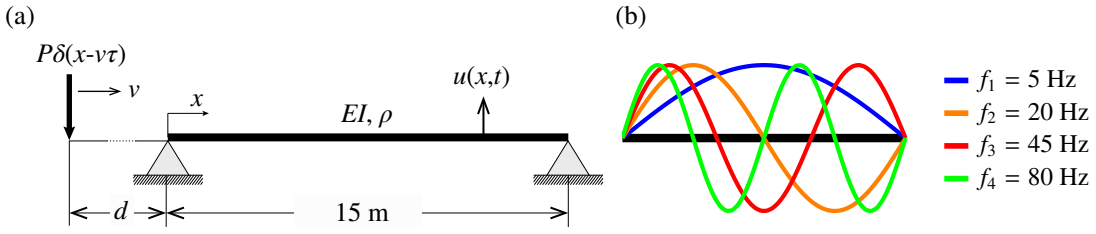

Figure 4: Geometry and mechanical properties of a simply supported beam with constant cross-section and traversed by a single moving load (a), and modal properties of the beam (b).

5.1.1. Analytical solution

In order to serve as a validation basis for the proposed HTSA approach, the analytic solution to the moving load problem of a simply supported beam is concisely derived. Neglecting damping effects, the differential equation of vertical displacements $u(x,\tau)$ of an Euler-Bernoulli beam under a moving load reads:

$$\rho(x)\frac{\partial^2 u(x,\tau)}{\partial \tau^2} + \frac{\partial^2}{\partial x^2}\left[EI(x)\frac{\partial^2 u(x,\tau)}{\partial x^2}\right] + P\delta(x - v\tau) = 0, \tag{31}$$

with $\tau = t - d/v$ being the relative time. Assuming that the system behaves linearly, the solution of Eq. (31) can be obtained by applying modal decomposition. That is, $u(x,\tau) = \mathbf{\Phi}(x)\mathbf{y}(\tau)$, with $\mathbf{\Phi}(x)$ being the modal matrix containing the mode shapes $\Phi_n(x)$ of the beam by columns, and $\mathbf{y}(\tau)$ the vector of modal displacements. In virtue of the orthogonality property of the mode shapes, Eq. (31) can be decoupled into modal coordinates $y_n(\tau)$ as:

$$\int_0^L \Phi_n(x)\left[\rho(x)\frac{\partial^2 y_n(\tau)}{\partial \tau^2}\right]\Phi_n(x)\mathrm{d}x + \int_0^L \frac{\partial^2 \Phi_n(x)}{\partial x^2}EI(x)\frac{\partial^2 \Phi_n(x)}{\partial x^2}y_n(\tau)\mathrm{d}x + P\Phi_n(v\tau) = 0. \tag{32}$$

From Eq. (32), the generalized mass M_n and stiffness K_n values associated with the n-th mode can be identified as:

$$M_n = \int_0^L \Phi_n(x)\rho(x)\Phi_n(x)\mathrm{d}x, \quad K_n = \int_0^L \frac{\partial^2 \Phi_n(x)}{\partial x^2}EI(x)\frac{\partial^2 \Phi_n(x)}{\partial x^2}\mathrm{d}x. \tag{33}$$

At this point, it is possible to include the damping effects by means of a modal damping ratio ζ_n. Using dot notation to represent time derivatives, Eq. (32) can be rewritten in a more compact form as:

$$\ddot{y}_n(\tau) + 2\zeta_n\omega_n\dot{y}_n(\tau) + \omega_n^2 y_n(y) + (P/M_n)\,\Phi_n(v\tau) = 0. \tag{34}$$

The homogeneous solution of Eq. (34) can be readily derived as:

$$y_n^h(\tau) = e^{-\zeta_n\omega_n\tau}\left[A_n\cos\left(\omega_n^d\tau\right) + B_n\sin\left(\omega_n^d\tau\right)\right], \tag{35}$$

where terms A_n and B_n are constants to be determined by the boundary conditions. Terms ω_n and Φ_n denote the undamped angular frequency and mode shape of the n-th vibration mode and are given by:

$$\omega_n = n^2\pi^2\sqrt{\frac{EI}{\rho L^4}}, \quad \Phi_n(x) = \sin\left(\frac{n\pi x}{L}\right). \tag{36}$$

The resulting natural frequencies $f_n = \omega_n/2\pi$ and mode shapes of the first four vibration modes of the present case study are depicted in Fig. 4 (b).

Defining the following non-dimensional parameters:

$$\Omega = n\pi(v\tau)/L, \quad S_n = \Omega/\omega_n, \quad \eta = \frac{2PL^2}{EIn^4\pi^4}\left[\left(1 - S_n^2\right)^2 + 4\left(\zeta_n S_n\right)^2\right]^{-1}, \tag{37}$$

the particular solution of Eq. (31) reads:

$$y_n^p(\tau) = C_n\cos(\Omega\tau) + D_n\sin(\Omega\tau), \tag{38}$$

with C_n and D_n given by:

$$C_n = -2\zeta_n\eta L, \quad D_n = \left(1 - S_n^2\right)\eta L. \tag{39}$$

In this light, the solution of the modal coordinate $y_n(\tau)$ is obtained as $y_n(\tau) = y_n^p(\tau) + y_n^h(\tau)$, and terms A_n and B_n in Eq. (35) are found by applying the simply supported boundary conditions, which leads to:

$$A_n = -C_n, \quad B_n = \frac{\zeta_n\omega_n C_n + \omega_n^d}{\omega_n^d}. \tag{40}$$

Considering that the dynamic response is governed by m vibration modes, the solution reads:

$$u(x,\tau) = \sum_{n=1}^{m}\left\{e^{-\zeta_n\omega_n\tau}\left[A_n\cos\left(\omega_n^d\tau\right) + B_n\sin\left(\omega_n^d\tau\right)\right] + C_n\cos(\Omega\tau) + D_n\sin(\Omega\tau)\right\}\Phi_n(x). \tag{41}$$

Since the system is assumed to be linear, the previous formulation can be readily extended to general train compositions by means of linear superposition.

5.1.2. Hilbert transform of the analytical solution

In order to benchmark the instantaneous envelopes obtained by the HTSA model, the HT of the previous analytic solution is extracted following a similar procedure to the one formerly introduced in Section 4.2. In this case, the indefinite integrals involved in the HT of the homogeneous and particular solutions in Eqs. (35) and (38) can be obtained in closed-form as:

$$Y_n^h(\tau, s) = e^{-\zeta_n \omega_n |\tau|} \left\{ \mathrm{Si}\left(\omega_n^d (s-\tau)\right) \left[A_n \sin\left(\omega_n^d \tau\right) - B_n \cos\left(\omega_n^d \tau\right) \right] - \mathrm{Ci}\left(\omega_n^d (s-\tau)\right) \left[A_n \cos\left(\omega_n^d \tau\right) + B_n \sin\left(\omega_n^d \tau\right) \right] \right\}, \tag{42}$$

$$Y_n^p(\tau, s) = \mathrm{Si}\left(\omega_n^d (s-\tau)\right) \left[C_n \sin\left(\omega_n^d \tau\right) - D_n \cos\left(\omega_n^d \tau\right) \right] - \mathrm{Ci}\left(\omega_n^d (s-\tau)\right) \left[C_n \cos\left(\omega_n^d \tau\right) + D_n \sin\left(\omega_n^d \tau\right) \right]. \tag{43}$$

Note that, similarly to Eq. (16), the relative time in the exponential term of Eq. (42) is included in absolute value to impose a mirroring around $\tau = 0$. On this basis, the HT of the analytic solution can be obtained in the Cauchy principal value sense by applying similar limits to those previously presented in Eqs. (20) and (23), that is:

$$\tilde{y}_n(\tau) = \frac{1}{\pi} \left\{ \lim_{s \to L-\varepsilon} \left[Y_n^h(\tau, s) + Y_n^p(\tau, s) \right] - \lim_{s \to \varepsilon} \left[Y_n^h(\tau, s) + Y_n^p(\tau, s) \right] + \lim_{s \to \infty} \left[Y_n^h(\tau, s) \right] - \lim_{s \to \varepsilon} \left[Y_n^h(\tau, s) \right] \right\}. \tag{44}$$

5.1.3. Validation results

Two different load cases have been studied, namely (i) one single moving load in Fig. 5, and (ii) the 56 axles ICE2 train in Fig. 6 (the train composition is given in [52]). In these analyses, the first four vibration modes depicted in Fig. 4 (b) have been considered.

The first load case consists of a single moving load of 100 kN crossing the beam at 150 km/h, and originally located $d = 50$ m far from the origin. The displacement and acceleration time series computed at the mid-span of the beam are shown in Figs. 5 (a) and (b), respectively. In these figures, the solution obtained by the semi-analytic approach (overviewed in Section 3 and labelled with FS) is depicted alongside the analytic solution previously derived in Section 5.1.1. Firstly, it is noted that the instantaneous envelopes obtained by the proposed HTSA approach perfectly overlap those computed with the analytic solution. In this validation case study, the complete HTSA model presented in Sections 4.2 and 4.3 is employed without including any of the computational reduction strategies reported in Section 4.4. The effect of the mirroring included in the exponential terms in Eqs. (16) and (42) is evident in the time period $0 < t < 1.3$ s ($\tau < 0$) before the load enters the structure. Such a mirroring provides a smooth transition at the entrance of the loads and avoids the appearance of jump discontinuities, which is particularly critical for train compositions comprising multiple axle loads.

Figures 6 (a) and (b) show, respectively, the displacement and acceleration time series at mid-span of the beam under the passage of the ICE2 train at 160 km/h. Perfect overlapping can be also noted herein between the instantaneous envelopes obtained by the analytic solution and the HTSA approach, which demonstrates the correctness of the presenting HTSA approach for mono- and multi-axle moving loads.

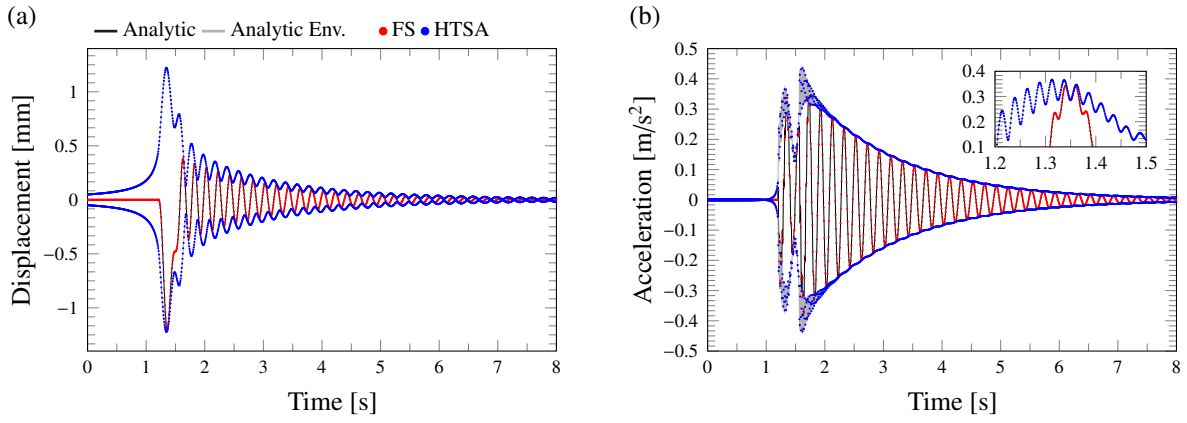

Figure 5: Displacement (a) and acceleration (b) time series at mid-span of a simply supported beam traversed by a single moving load of 100 kN travelling at 150 km/h and starting 50 m far from the origin of the beam ($\Delta t = 1$ ms).

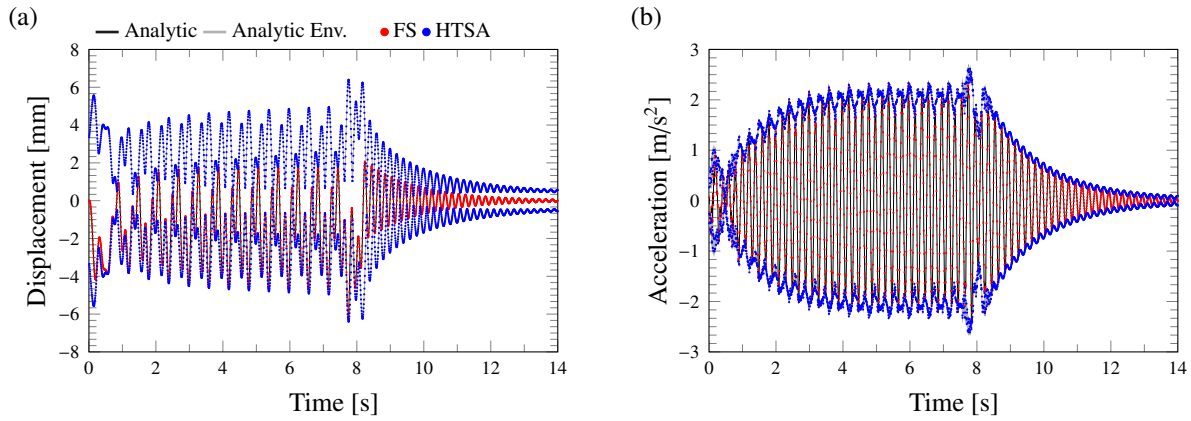

Figure 6: Displacement and acceleration series at mid-span of a simply supported beam traversed by the ICE2 train travelling at 160 km/h (Δt = 1 ms).

5.2. Case study II: Continuous three-span bridge from Eurocode 1.

The second case study is a continuous three-span high-speed bridge analysed in Eurocode 1 [5]. The geometry of the bridge is sketched in Fig. 7, which consists of two 25 m long outer spans and a 30 m long central one. The bridge has been modelled in the commercial FEM code SAP2000 with 8 Euler-Bernoulli beam elements per span. The bridge has a constant mass per unit length ρA=14435.25 kg/m, flexural stiffness EI=110649.6 MNm^2, and constant modal damping ratio of ζ=1%. Five vibration modes with resonant frequencies below 30 Hz have been found by linear modal analysis of the FEM (see Fig. 7), which are considered in the subsequent analyses. With regard to the loading conditions, the dynamic response of the bridge has been studied under the passage of the A1 train of the HSML-A model of Eurocode at two different speeds, namely v = 150 km/h and v = 277 km/h. The first speed is non-resonant, so the response is expected to be governed by all the considered modes of vibration. Conversely, the second speed induces the resonance of the first mode of frequency f_1 = 4.3 Hz.

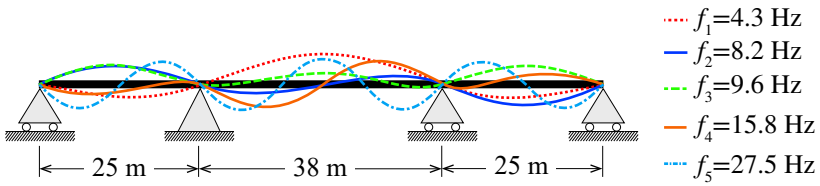

Figure 7: Continuous three-span bridge proposed in Eurocode 1 [5].

This case study is primarily aimed at assessing the effectiveness of the reduced HT through window filtering previously proposed in Eq. (29) in Section 4.4. To do so, three different integration windows have been considered, namely d_i = 28.1 m, 9.4 m and 3.1 m, and the results have been benchmarked against the complete HT considering the whole time domain. In these analyses, the infinite extension approximation of the homogeneous solution from Eq. (30) has been considered for the vibration modes with resonant frequencies above 10 Hz, that is the fourth and the fifth modes (see Fig. 7). In addition, the dynamic analyses have been conducted considering a time stepping of $\Delta t = T_{min}/10$, with $T_{min} = 1/27.5$ s being the minimum period of all the vibration modes included in the analysis.

Figures 8 and 9 show the displacement and acceleration time series at mid-span of the central span for train speeds of 150 km/h and 277 km/h, respectively. Firstly, let us focus on the instantaneous envelopes of displacement in Fig. 8. In the very first range of forced vibrations (0-1.5 s), it can be noted that the demodulation capability of the reduced HT considerably decreases as shorter window lengths are utilized. This is ascribed to errors stemming from the truncation of signal components in the range of negative relative times ($\tau < 0$), where the mirroring operation in Eq. (16) is activated. When using shorter window lengths, the contribution of those loads that have not entered the structure yet (i.e. those with $\tau < 0$) is excluded from the demodulation if $|\tau| < d_i/2v$, making the instantaneous envelopes progressively approach the original time series. In the last part of free vibrations, it is observed that shorter integration windows make the envelopes tend to the HT of the solution considering the infinite extension simplification in Eq. (30). In these cases, the contribution of the semi-analytic solution inside the bridge ($l_k/v < t < l_k/v + L/v$) losses importance and the reduced HT only accounts for the integration of the homogeneous solution. It is important to note that the use of reduced HTs with too short integration windows may lead to considerable jump discontinuities, as it is the case of the window length d_i = 3.1 m. Since the

mean axle separation of the A1 train is 8.11 m, such a short integration window fails to represent the contribution of consecutive axles. Nevertheless, the appearance of jump discontinuities is minimized with moderate window lengths such as d_i = 28.1 m and 9.4 m, which do account for the contribution of consecutive axles. With regard to the envelopes obtained for the resonant speed of 277 km/h in Fig. 9, similar conclusions can be extracted, although it is evident that the jump discontinuities for the window length d_i = 3.1 m are less influential. In this case, the jump discontinuities are primarily due to poor demodulation of the modal coordinate of the fundamental vibration mode (f_1 = 4.3 Hz). Conversely, the previous case of non-resonant train speed is characterized by the contribution of several vibration modes, thereby the demodulation errors induced by the reduced HT add up for all the modal coordinates involved in the response.

Finally, Fig. 10 presents the computational times required by the HTSA model to obtain the instantaneous envelopes previously reported in Figs. 8 and 9. As expected, the computational time increases exponentially with the length of the integration window due to the associated increase of the number of load elements to be included in the HT at every time step. Therefore, the choice of the window length must pursue a compromise between demodulation capability and computational cost. In light of the previous analyses, the average separation between the train axles provides a suitable initial guess of the window length.

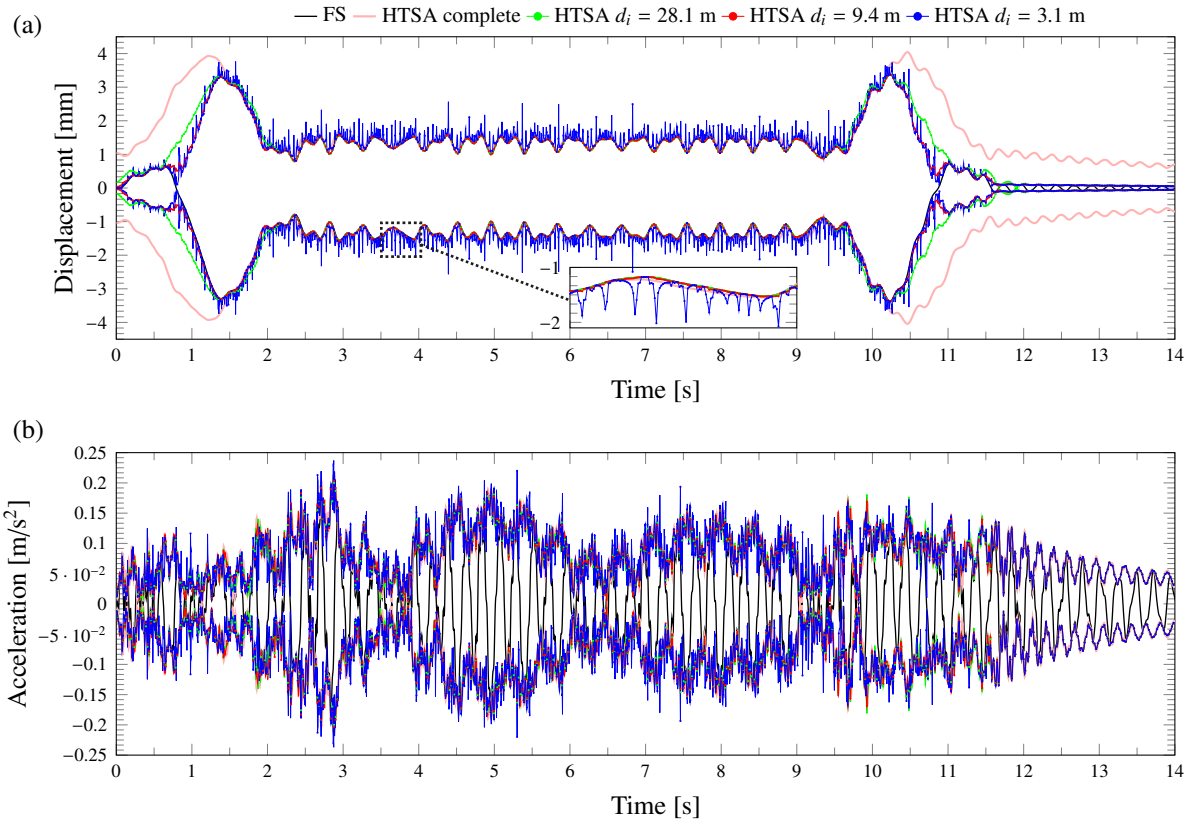

Figure 8: Displacement (a) and acceleration (b) time series and instantaneous envelopes at mid-span of the central span of the continuous three-span bridge traversed by the A1 train of the HSML-A model of Eurocode 1 at 150 km/h ($\Delta_t = T_{min}/10$).

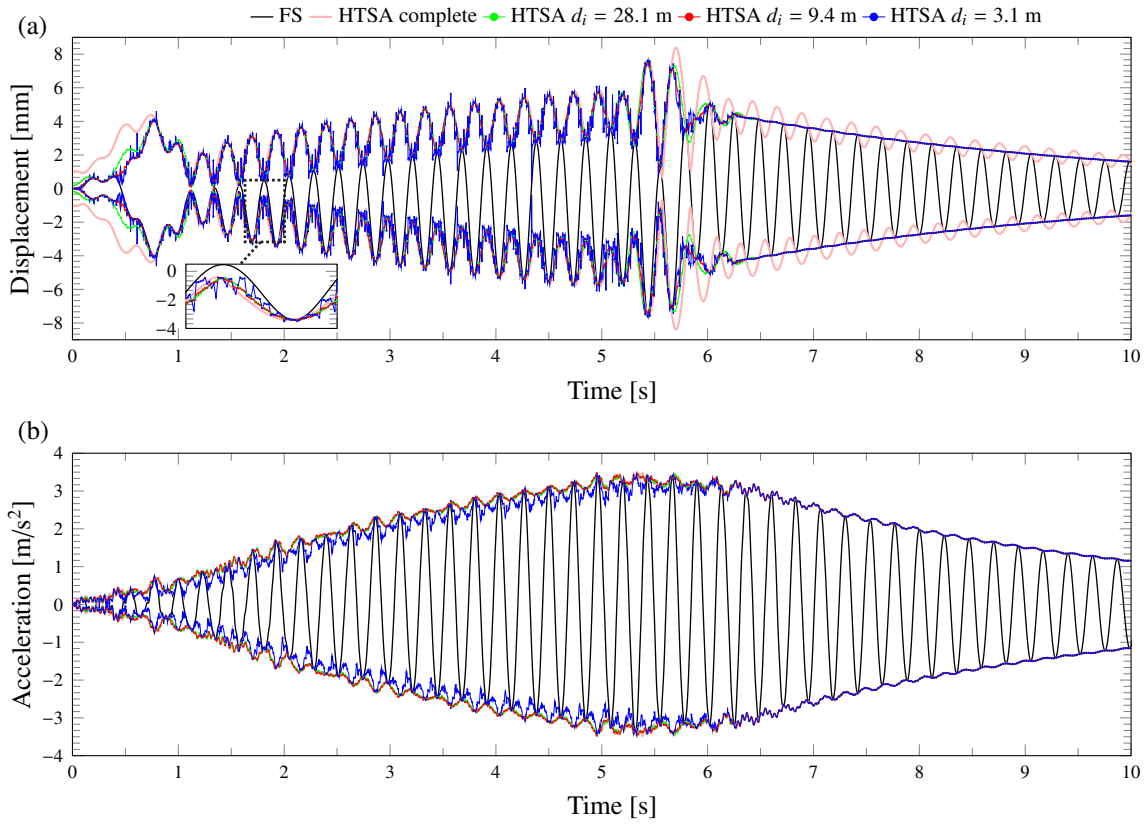

Figure 9: Displacement (a) and acceleration (b) time series and instantaneous envelopes at mid-span of the central span of the continuous three-span bridge traversed by the A1 train of the HSML-A model of Eurocode 1 at 277 km/h ($\Delta_t = T_{min}/10$).

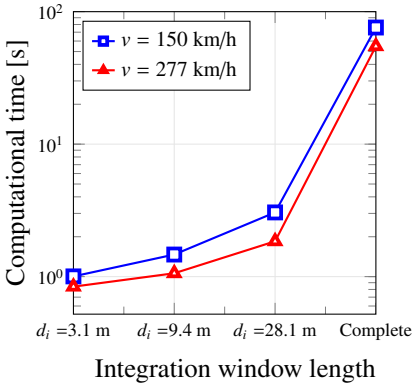

Figure 10: Computational time versus window lengths of the instantaneous displacement and acceleration envelopes computed by the HTSA model for a continuous three-span bridge traversed by the A1 train of the HSML-A model of Eurocode 1 ($\Delta t = T_{min}/10$).

5.3. Case study III: concrete box girder bridge, the viaduct of Rodenillo.

This case study consists of a 3D double-track U-shaped girder high-speed railway bridge, the viaduct of Rodenillo. The main aim of this case study is to appraise the effectiveness of the proposed HTSA meta-model in terms of accuracy and computational efficiency when applied to a realistic moderate-damped bridge model.

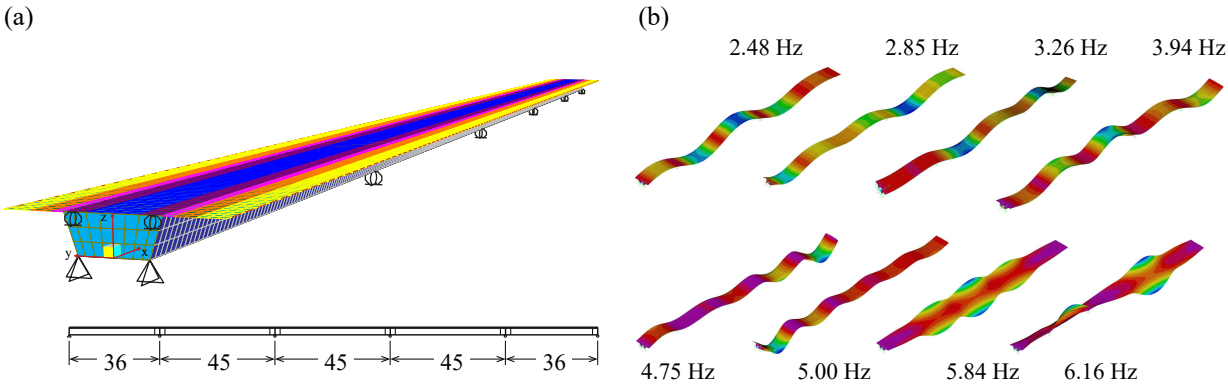

Figure 11: Lateral view and FEM of the viaduct of Rodenillo (a), and first eight vibration modes (b) (Units in m).

The viaduct of Rodenillo is a cast-in-place concrete post-tensioned box-girder bridge located in the HSR line Madrid-Valencia in Spain. It comprises five continuous spans with a total length of 207 m, including two 36 m long outer spans and three 45 m long central spans (see Fig. 11 (a)). The bridge has a single-cell box cross-section with a depth of 3.1 m with 3.9 m long cantilevers on both sides, defining a 14 m wide concrete deck. The viaduct has been modelled in the commercial FEM code SAP2000 using shell elements (see Fig. 11 (a)). The train loads have been applied in the centreline of one of the railway tracks 2.265 m far from the centre of the deck. The modal features of the bridge have been obtained by linear modal analysis of the FEM, finding a total of 123 modes of vibration with resonant frequencies below 30 Hz that must be considered in the subsequent dynamic analyses. Figure 11 (b) shows the first eight modes of vibration. These include one first, two second and one third order bending modes of frequencies 2.48 Hz, 2.85 Hz, 3.26 Hz and 3.94 Hz, respectively, local bending modes of frequencies 4.75 Hz and 5.00 Hz, and first and second order torsion modes of frequencies 5.84 Hz and 6.16 Hz, respectively. A constant modal damping ratio of ζ=2% is selected according to the Spanish code IAPF-07 [52]. This case study was previously analysed in our previous work in [22], where interested readers may find further details on the structure and the FEM.

5.3.1. Dynamic analysis results

The dynamic response of the viaduct has been computed at 45 different post-processing points on the deck for the ten trains of the HSML-A model of Eurocode. These include points located at centre-line and at the edges of the ballast bed for every quarter- and mid-span. Nevertheless, because of space constraints, only a few representative results are shown herein. Readers are encouraged to consult the supplementary material if interested in the complete analysis.

Firstly, Fig. 12 reports a parametric analysis conducted in order to identify a suitable integration window for the HTSA model. To do so, instantaneous envelopes of acceleration and displacement time series have been obtained for four different window lengths, namely d_i = 3 m, 9 m, 21 m, and 63 m. The analysis has been applied to the dynamic response of the viaduct of Rodenillo under the passage of the A1 train of the HSML-A model at 307 km/h. This speed originates the resonance of the fifth vibration mode, which defines a local bending mode with frequency of 4.75 Hz (see Fig. 11 (b)). In all the subsequent results, the infinite extension approximation of the homogeneous solution from Eq. (30) has been considered for all the vibration modes with resonant frequencies above 10 Hz. The reported results correspond to the dynamic response of the bridge at the edge of the ballast layer at mid-span of the central span, and the time series have been obtained with a time stepping of $\Delta t = T_{min}/10 = 3.33$ ms. In a similar way to the results previously reported in Figs. 8 and 9, a window length of d_i = 3 m leads to severe jump discontinuities due to its inability to account for the contribution of consecutive axle loads. On the other hand, the integration windows of d_i = 9 m, and 21 m show minimum differences with respect to the case of d_i = 63 m (which mostly resembles the complete HT), specially in terms of acceleration envelopes in Fig. 12 (b). Some differences can be noted in the displacement envelopes in Fig. 12 (a), particularly in the first part of forced vibrations ($0 < t < 2.5$ s). In this case, it is observed that the window length d_i = 63 m yields a better demodulation of the signals, while the instantaneous envelopes obtained for the windows d_i = 9 m and d_i = 21 m approach the semi-analytic solution (FS). In view of these results, the definition of the integration window length as at least the average axle separation can be stated as a general recommendation. Nonetheless, it is important to remark that the computational cost involved in a sensitivity analysis similar to the one reported in Fig. 12 is not very high. This allows tailoring the window length for every case study, which can be kept constant in the subsequent computation of the maximum response design envelopes, being the latter the true computational bottleneck in this problem. In

this particular case study, an integration window length of $d_i = 9$ m is chosen hereafter as a compromise between accuracy and computational cost.

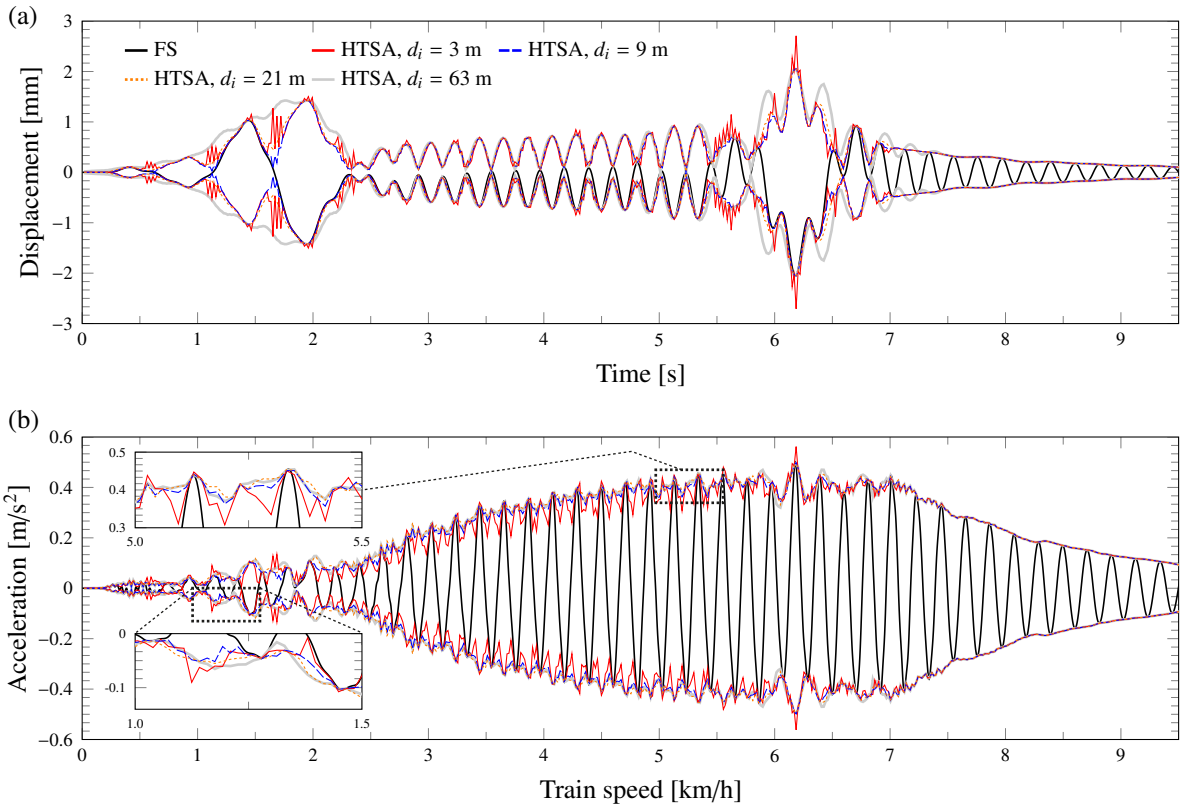

Figure 12: Displacement (a), acceleration (b) and instantaneous envelope time-series computed at the edge of the ballast layer at mid-span of the central span of the viaduct of Rodenillo (Train A1 of the HSML-A model of Eurocode, $v = 307$ km/h, $\Delta t = T_{min}/10$).

Figures 13 (a) and (b) show the maximum absolute displacement and acceleration envelopes, respectively, as functions of train speed under the passage of the A1 train of the HSML-A model of Eurocode 1. In order to evaluate the effectiveness of the proposed HTSA meta-model, four different sampling time steps are selected, namely $\Delta t = T_{min}/5$, $T_{min}/2$, T_{min} and $2T_{min}$. As a benchmark result, the forward solution obtained by the semi-analytic method (FS) with a sampling time step of $\Delta t = T_{min}/10$ is also presented. In the analyses, a free vibration time of six times the highest period of the bridge has been included, and the range of train speeds of 20-420 km/h has been sampled with speed increments of 1 km/h. It is observed that, either in terms of displacements or accelerations, the HTSA model provides estimates of the design envelopes very close to the FS when time sampling rates of $\Delta t = T_{min}/5$, $T_{min}/2$, and T_{min} are selected. Conversely, substantial errors can be observed in the case of the design envelopes computed with $\Delta t = 2T_{min}$. In particular, it is interesting to note that the errors are larger in terms of displacements and increase with train speed. This behaviour can be explained by the results previously reported in Fig. 12, where the presence of oscillating components was shown more important in terms of acceleration and, as a result, the demodulation by the HTSA approach is more effective in this case. Additionally, as an evidence of the demodulation limitations arising in reduced Hilbert integration schemes, the results in Fig. 12 also showed that a certain oscillating behaviour remains in the instantaneous envelopes. Therefore, too large time steps may lead to substantial sampling errors as reported in Fig. 13, specially for high train speeds activating high-frequency modes. Similar conclusions can be extracted when studying the global design envelopes for the ten trains of the HSML-A model in Fig. 14.

In light of the results above, an in-depth analysis of the efficiency of the HTSA meta-model has been performed in terms of computational time and accuracy, and the results are summarized in Fig. 15. In this figure, errors in the estimation of the design acceleration/displacement design envelopes are presented in the shape of mean and root-mean-squared (rms) differences, and relative errors in the estimation of global maxima. To do so, the forward solution with time stepping of $\Delta t = T_{min}/10$ is assumed to yield the true design envelopes. It is noted in Fig. 15 (a) that, compared to the reference solution, the proposed HTSA model begins to be competitive in terms of computational time for time sampling steps about above $\Delta t = T_{min}/2$. Furthermore, the rms errors depicted in

Figs. 15 (b) and (c) demonstrate that the HTSA model is considerably less sensitive to decreases in the time sampling frequency than the forward solution. Interestingly, it is noted that the FS model leads to smaller rms errors to those obtained with the HTSA model for time steps below $\Delta t = T_{min}/2$ and $\Delta t = T_{min}/2$ in terms of maximum acceleration and displacement design envelopes, respectively. This is due to the fact that the HTSA model provides, by definition, equal or larger estimates to those obtained by the FS model with identical time evaluation steps. This feature can be confirmed when inspecting the mean errors in Figs. 15 (b) and (c). It is noted that the FS model yields monotonically increasing negative mean errors (i.e. underestimations of the true design envelopes), while the HTSA model provides positive values (i.e. overestimations) for time steps up to $\Delta t = T_{min}$. From these analyses, a suitable time sampling step for the HTSA model can be set as $\Delta t = T_{min}$, which reaches a reduction in the computational time of about 45% with limited relative errors in the estimation of the global maximum acceleration and displacement of -1.17% and +0.17%, respectively.

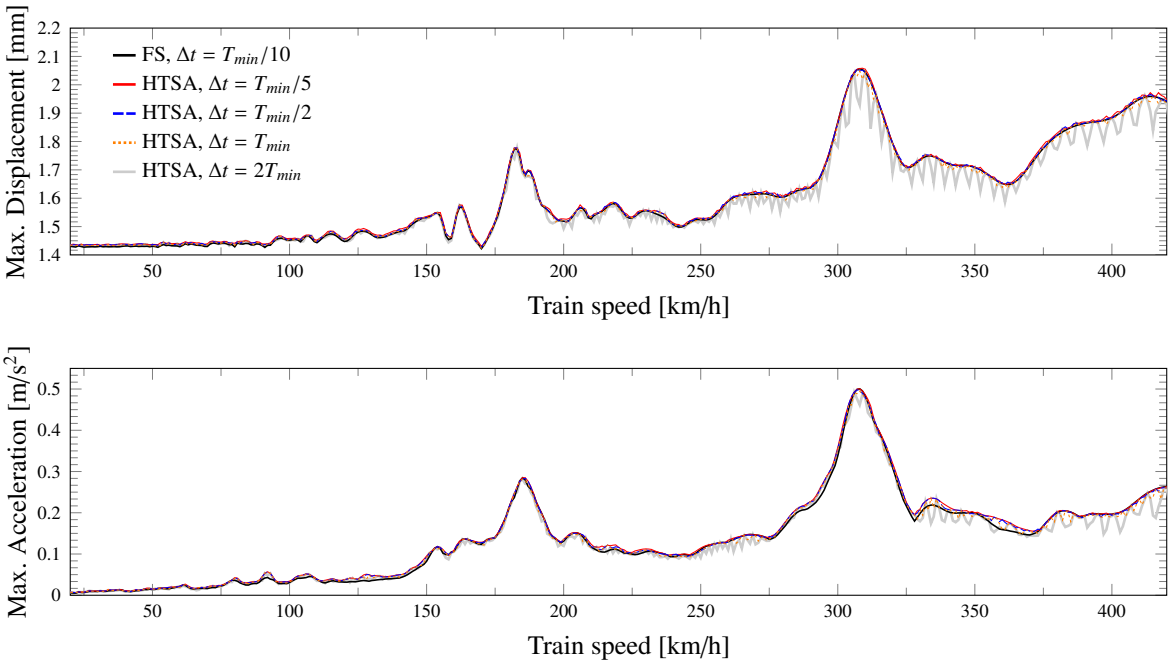

Figure 13: Maximum absolute envelopes of displacements (a) and accelerations (b) of the viaduct of Rodenillo as functions of the train speed considering different time sampling rates. Displacements and accelerations are computed at the edge of the ballast layer at mid-span of the central span of the viaduct of Rodenillo (Train A1 of the HSML-A model of Eurocode, d_i = 9 m).

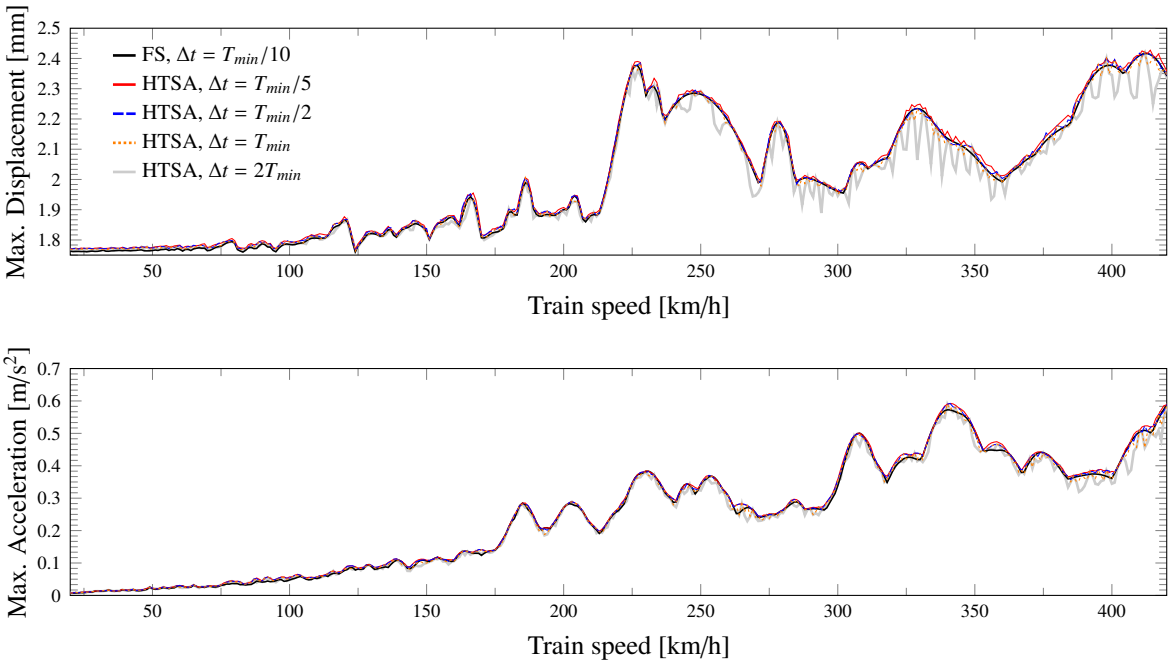

Figure 14: Maximum absolute envelopes of displacements (a) and accelerations (b) of the viaduct of Rodenillo as functions of the train speed considering different time sampling rates. Displacements and accelerations are computed at the edge of the ballast layer at mid-span of the central span of the viaduct of Rodenillo (Ten trains of the HSML-A model of Eurocode, d_i = 9 m).

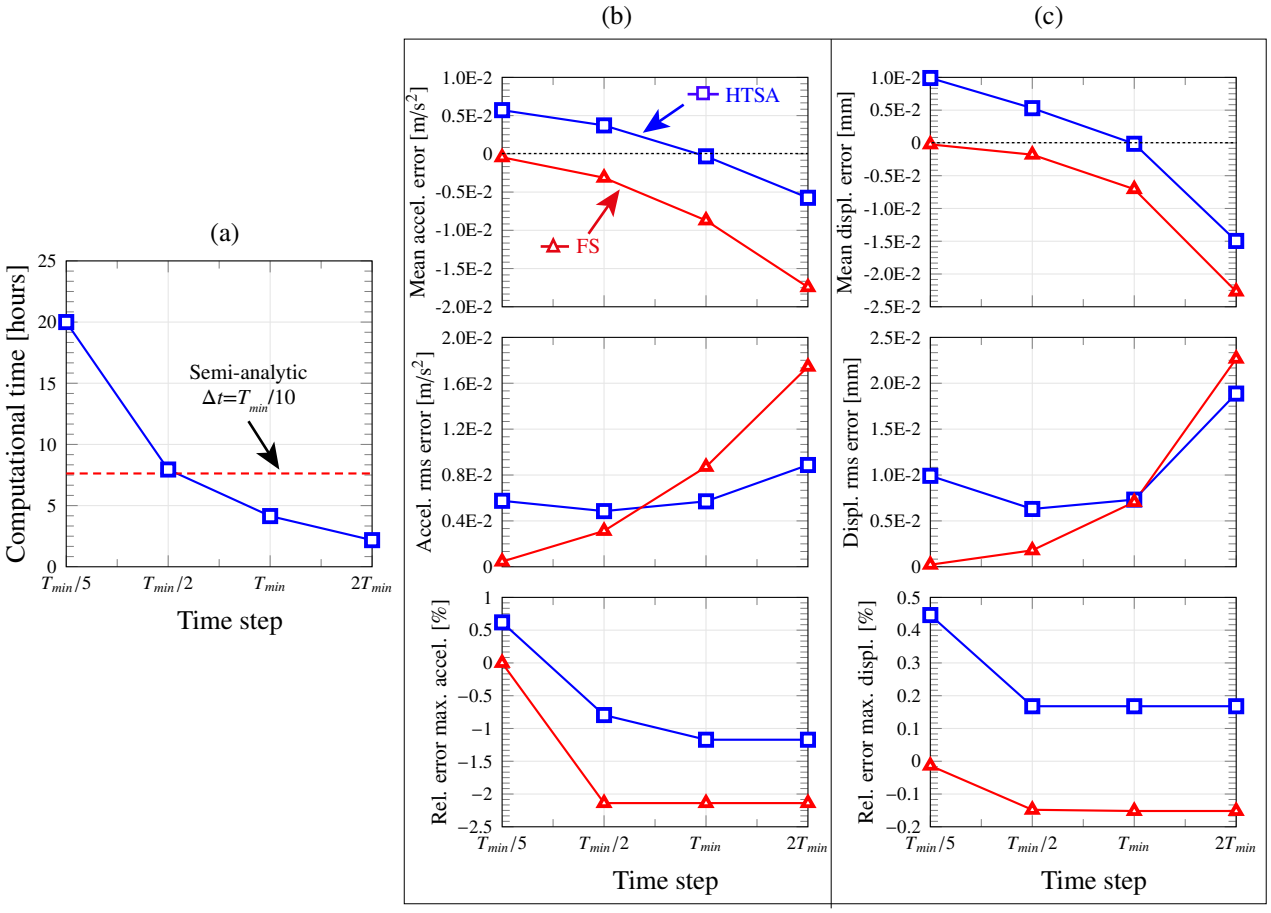

Figure 15: Computational time (a) and prediction errors in terms of acceleration (b) and displacement design envelopes (c) versus time sampling steps for the HTSA meta-model applied to the viaduct of Rodenillo.

5.4. Case study IV: bowstring-arch composite steel-concrete bridge, the viaduct of Santa Ana.

This last case study copes with the dynamic analysis of a 3D composite steel-concrete bridge, the viaduct of Santa Ana. Specifically, the aim of the results presented hereafter is to evaluate the efficiency of the proposed HTSA approach in terms of computational cost and efficiency for a low-damped bridge structure.

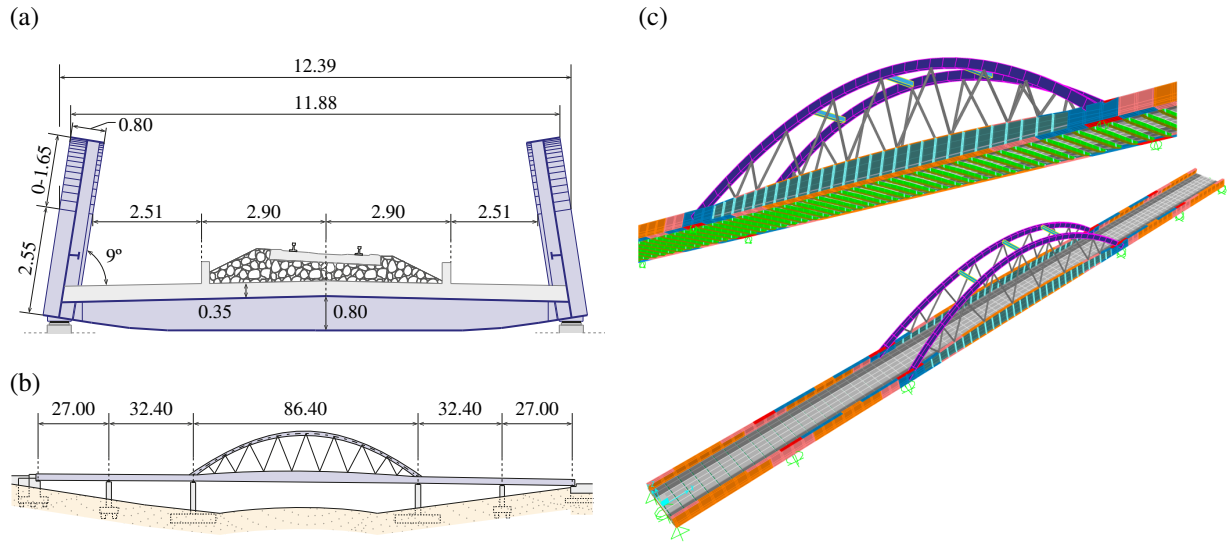

Figure 16: Cross-section (a), lateral view (b), and FEM of the viaduct of Santa Ana (c) (Units in m).

The viaduct of Santa Ana is located in the still under construction Huelva-Almería HSL Andalusian Transverse

Axis in Spain, and crosses the Córdoba-Málaga HSL close to the town of Santa Ana. The viaduct is a five-span composite steel-concrete bridge, including four outer spans of 32.4 m and 27.0 m, and a central 86.4 m long bow-string span (see Fig. 16 (a)). The bridge is defined with an inverted U cross-section of 12.40 m width, comprising two continuous I-shaped steel plate girders, transverse steel floorbeams, and a 0.35 m thick concrete deck cast on profiled steel sheets. The longitudinal girders have a constant height of 2.55 m in the outer spans, and a variable height between 2.55 m and 4.20 m in the central one according to a parabolic profile. The central span of the viaduct is characterized by two parabolic steel arches with a maximum rise of 17.0 m. These are defined with steel beams with box cross-section of 0.80 m $\times$ 1.5 m $\times$ 2.5 cm, and are tied to the longitudinal girders by a lattice of tubular hangers with outer diameter 0.4 m and wall thickness 2 cm. The longitudinal girders and the arches are inclined at 9° with respect to the vertical. Finally, the superstructure of the track consists of a single UIC-60 rail, prestressed concrete sleepers and a 0.50 m thick ballast bed. Further technical information of the structure, including its design details and construction process, can be found in reference [53].

5.4.1. Finite element model

In order to extract the modal features of the structure, the viaduct has been modelled in the commercial FEM code SAP2000 (see Fig. 16 (c)). To do so, shell elements have been used to model the steel girders, floorbeams and stiffeners, including up to fourteen different sections with thickness varying between 12 and 40 mm. The composite deck (concrete and profiled steel sheets) has been modelled with orthotropic shell elements. Beam elements have been used for the modelling of the arches, horizontal braces, and tubular hangers. In addition, massless infinitely rigid beam elements have been used to simulate the connection of the concrete deck and the steel ribs through shear studs. All in all, the number of elements used in the FEM amounts to 54660, including 810 beam and 53850 shell elements. The material properties used in the model are collected in Table 1. All the spans of the bridge are simply supported over plain elastomeric bearing pads, so the boundary conditions include fixed bearings at the first abutment and sliding bearings in the rest of supports. Additionally, vertical displacements are also constrained at the extremes of the rail to simulate the connection with the rest of the railway and avoid the appearance of fictitious impacts at the entrance of trains.

Table 1: Material properties used in the FEM of the viaduct of Santa Ana.

Item	Unit	Value
Per-unit-length mass of rails	kg/m	60.0
Mass of sleepers	kg	290.0
Mass density of ballast	kg/m^3	1800.0
Young's modulus of concrete	GPa	29.2
Poisson's ratio of concrete	-	0.2
Mass density of concrete	kg/m^3	2550.0
Young's modulus of steel girder	GPa	203.89
Poisson's ratio of steel girder	-	0.2
Mass density of steel girder	kg/m^3	9370.0
Young's modulus of steel hangers	GPa	165
Poisson's ratio of steel hangers	-	0.2
Mass density of steel hangers	kg/m^3	8000.0

The FEM has been used to extract the modal features of the bridge through a linear modal analysis in SAP2000. A total of 266 modes of vibration has been found with resonant frequencies below 30 Hz to be included in the subsequent dynamic analyses. Figure 17 furnishes the first eight modes of vibration of the viaduct. These include three local modes of the arches, namely a first-order mode of frequency 1.37 Hz, a second-order one of 2.36 Hz, and a third-order one of 4.03 Hz. First- and second-order bending modes can be also noted in Fig. 17 with resonant frequencies of 2.46 Hz and 2.83 Hz, respectively, as well as two local bending modes of the outer spans of frequencies 3.17 Hz and 3.26 Hz. Finally, a first-order torsion mode of the central span is also shown with a resonant frequency of 3.59 Hz. With regard to the damping of the structure, a constant modal damping ratio of ζ=0.5% has been selected according to the prescriptions of the Spanish code IAPF-07 [52] for steel-concrete composite bridges.

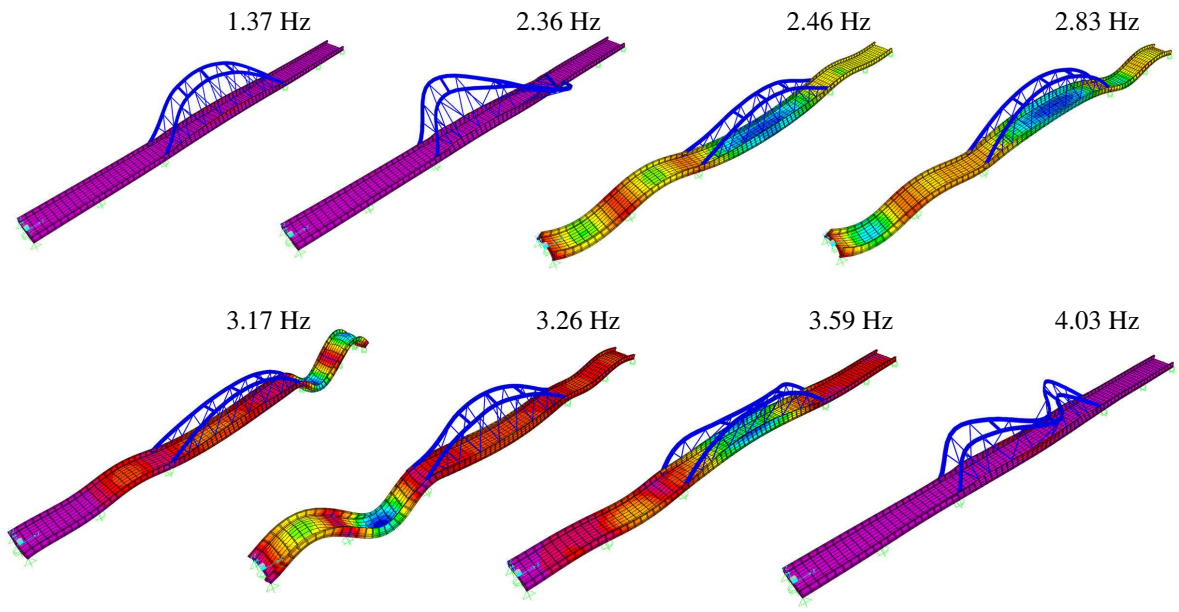

Figure 17: First eight vibration modes obtained by linear modal analysis of the FEM of the viaduct of Santa Ana.

5.4.2. Dynamic analysis results

In this case study, the dynamic response of the viaduct has been computed at 15 different post-processing points on the deck under the passage of the ten trains of the HSML-A model of Eurocode and two Spanish train compositions, namely the AVE and TALGO trains. Post-processing points have been located at every quarter and mid-span of the deck centre-line. Based upon an initial parametric analysis, similar to the one previously reported in the case study of the viaduct of Rodenillo, an integration window of 8.1 m has been selected for the HTSA meta-model. In this case study, the infinite extension approximation of the homogeneous solution from Eq. (30) has been also considered for all vibration modes with resonant frequencies above 10 Hz. Likewise the previous case study, readers can refer to the supplementary material for the complete analysis.

Figure 18 shows the instantaneous envelopes computed at the centre-line of the deck at mid-span of the central span under the passage of the A1 train of the HSML-A model at 187 km/h. This train speed corresponds to the resonance of the first bending mode with a frequency of 2.46 Hz (see Fig. 17). In order to illustrate the influence of the time sampling steps on the detection of maximum responses, the instantaneous envelopes have been computed considering different time steps, namely $\Delta t = T_{min}/5$, $T_{min}/2$, T_{min} and $2T_{min}$. Almost no discrepancies can be observed between the envelopes in terms of displacements in Fig. 18 (a). In this case, despite the reduction in the demodulation capability of the HTSA approach in the range of forced vibrations because of the adopted reduced Hilbert integration, the residual oscillating components in the instantaneous envelope can be accurately sampled with all the studied time steps. On the other hand, the acceleration time series in Fig. 18 (b) has essentially the shape of an oscillating signal. In this case, sampling errors in the instantaneous envelopes are more evident, specially in the surrounding of the absolute (global) maximum as shown in the zoom view in Fig. 18 (c).

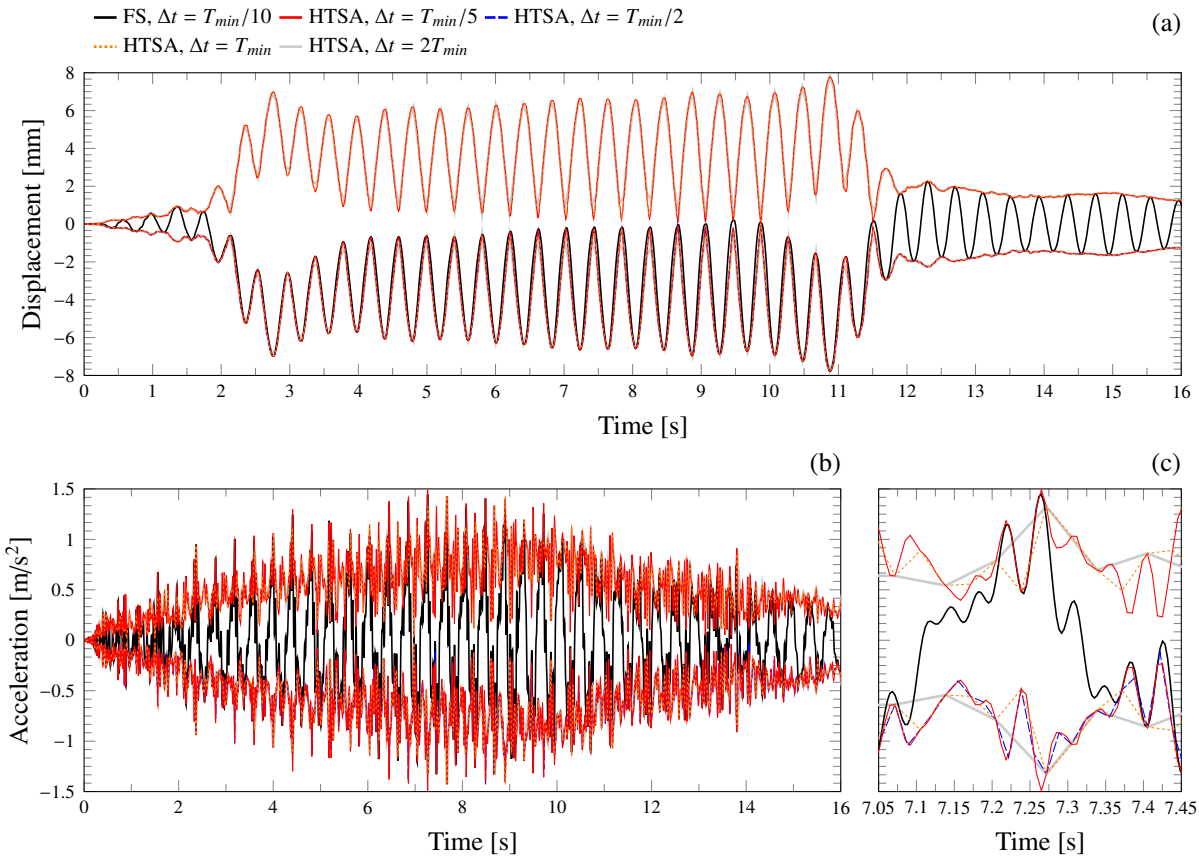

Figure 18: Displacement (a), acceleration (b) time-series and instantaneous envelopes computed at the centre-line of the deck at mid-span of the central span of the viaduct of Santa Ana. Zoom view of the region of maximum acceleration (c). (Train A1 of the HSML-A model of Eurocode, v = 187 km/h, d_i = 8.1 m).

Figures 19 (a) and (b) show the maximum absolute displacement and acceleration design envelopes, respectively, as functions of train speed under the passage of the A1 train of the HSML-A model. Moreover, Figs. 20 (a) and (b) show the counterpart results in terms of global design envelopes for the ten trains of HSML-A model and the AVE and TALGO trains. A free vibration time of six times the highest period of the bridge has been included in all the analysed time series, and the range of train speeds of 20-282 km/h has been sampled with speed steps of 1 km/h. It is important to indicate that the actual train speed range of the HSL where the bridge is inserted is limited to 20-235 km/h. Therefore, following the prescriptions by the Eurocode, the dynamic analysis must account for speeds up to 1.2 times the maximum train speed (i.e. $1.2 \cdot 235 = 282$ km/h). It is observed in Figs. 19 and 20 that, both in terms of displacements and accelerations, the HTSA model provides estimates of the design envelopes very close to the FS ($\Delta t = T_{min}/10$) when time sampling rates of $\Delta t = T_{min}/5$, $T_{min}/2$, and T_{min} are selected. Conversely, the design envelopes computed with $\Delta t = 2T_{min}$ report large underestimates of the global maximum response for some train speeds as a result of poor sampling limitations. Equivalent conclusions to those previously reported in the case study of the viaduct of Rodenillo can be extracted here on the distribution and origin of the sampling errors arising in the HTSA estimates.

Finally, the analysis of the computational efficiency of the HTSA meta-model is presented in Fig. 21. It can be noted in Fig. 21 (a) that, likewise the previous case study, the proposed HTSA meta-model begins to be computationally competitive compared to the forward solution for sampling time steps above $\Delta t = T_{min}/2$. With regard to the sensitivity of the HTSA meta-model to sampling frequency variations, Fig. 21 (b) shows monotonically increasing rms errors in terms of acceleration for decreasing sampling frequencies, which differs from the previous case study. This behaviour is ascribed to the contribution of high-frequency modes and the low damping of the bridge, which diminishes the demodulation capability of the HTSA approach. Nonetheless, the results in Figs. 21 (b) and (c) demonstrate that the sensitivity of the proposed HTSA approach to decreasing sampling frequencies remains considerably smaller than that of the forward solution. From these analyses, a suitable HTSA model can be defined with a sampling time step of $\Delta t = T_{min}$, which yields a reduction of the computational time of about 45.4% with limited relative errors in the detection of the global maximum acceleration and displacement of 1.64% and 0.17%, respectively.

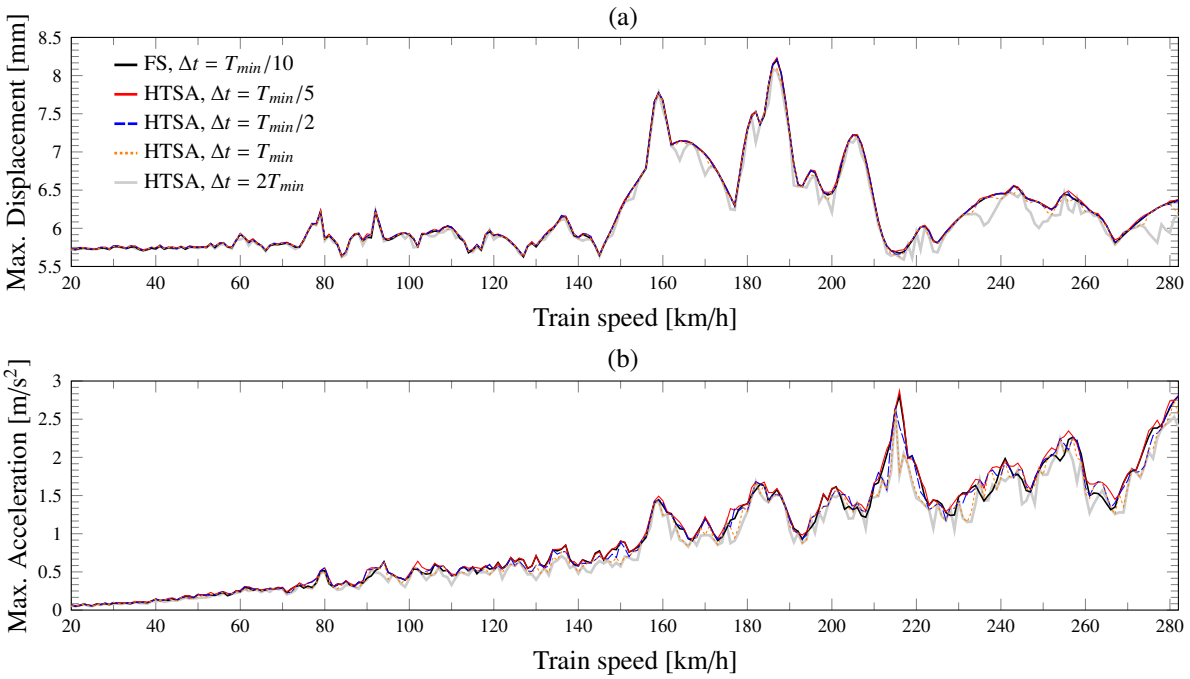

Figure 19: Maximum absolute envelopes of displacements (a) and accelerations (b) of the viaduct of Santa Ana as functions of the train speed considering different time sampling rates. Displacements and accelerations are computed at the edge of the ballast layer at mid-span of the central span of the viaduct of Santa Ana. (Train A1 of the HSML-A model of Eurocode, d_i = 8.1 m).

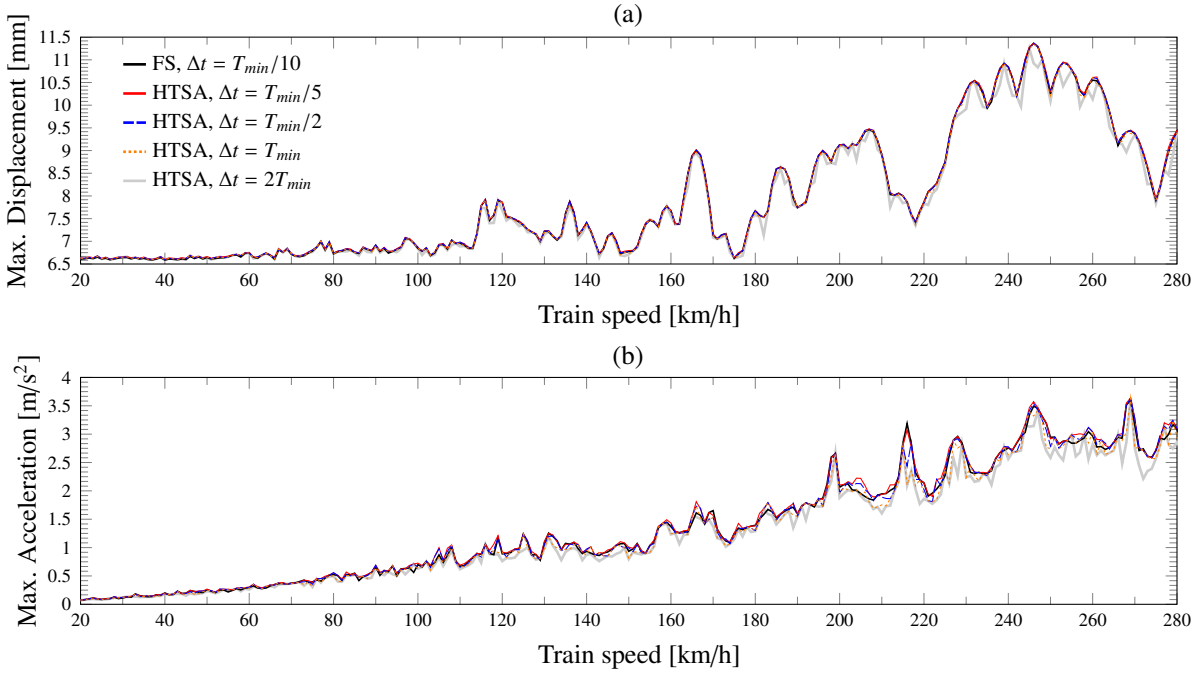

Figure 20: Maximum absolute envelopes of displacements (a) and accelerations (b) of the viaduct of Santa Ana as functions of the train speed considering different time sampling rates. Displacements and accelerations are computed at the edge of the ballast layer at mid-span of the central span of the viaduct of Santa Ana. (Ten trains of the HSML-A model of Eurocode, AVE and TALGO trains, d_i = 8.1 m).

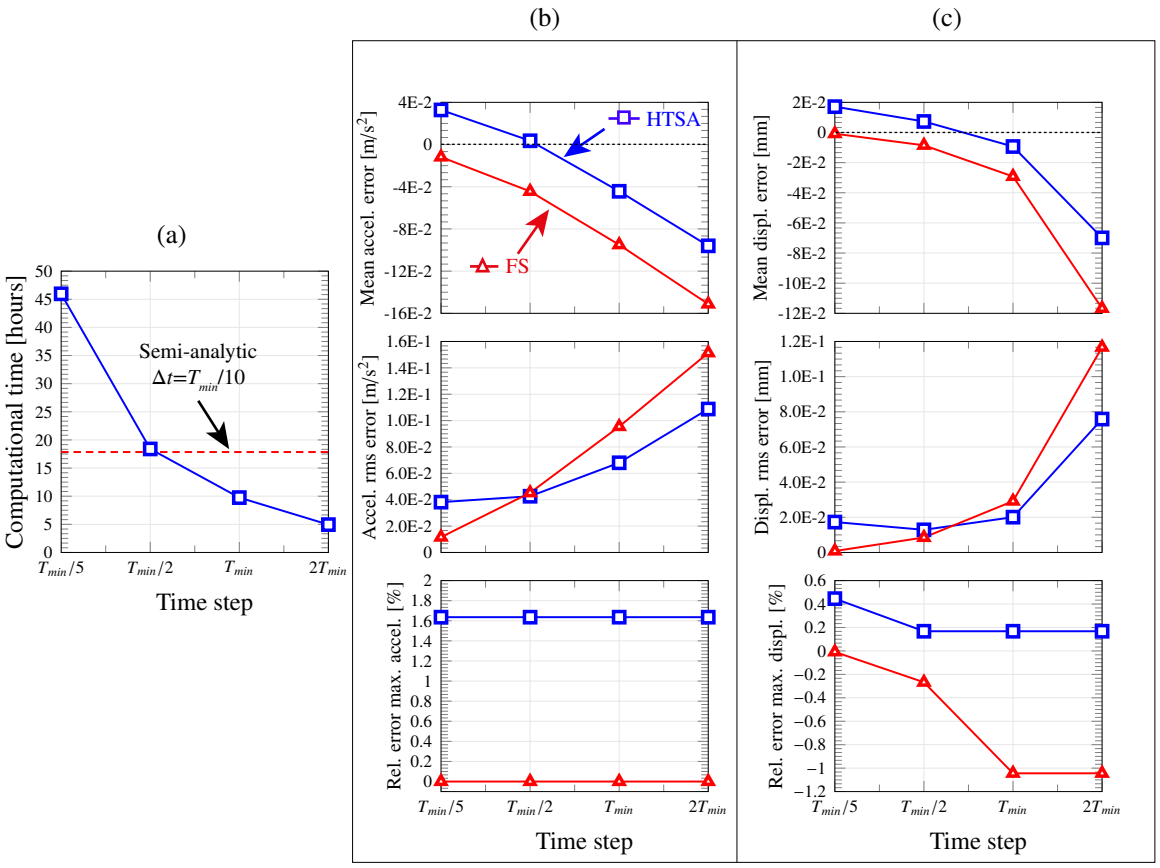

Figure 21: Computational time (a) and prediction errors in terms of acceleration (b) and displacement design envelopes (c) versus time sampling steps for the HTSA meta-model applied to the viaduct of Santa Ana.

6. Conclusions

This paper has proposed a novel meta-model for fast assessment of design envelopes of railway bridges. The proposed HTSA approach is based upon the HT of the semi-analytic solution for the moving-load problem of linear bridge structures. In virtue of the analytic definition of the semi-analytic method in the time-domain, the HT has been obtained in the Cauchy principal value sense in closed-form. In this way, the proposed HTSA model offers a suitable analytic framework for direct evaluation of instantaneous response envelopes. Since the oscillating components of dynamic response time series are minimized by the instantaneous envelope, the determination of global response maxima by the HTSA model has proved to have a low sensitivity to variations in the sampling frequency. Hence, design envelopes of railway bridges can be computed accurately by the proposed HTSA model with low sampling frequencies, achieving substantial reductions in computational time compared to the forward semi-analytic solution. In order to demonstrate the effectiveness of the proposed HTSA meta-model, four validation case studies have been presented, including two 1D and two realistic 3D bridge models. The main findings of this work can be summarized as follows:

- On the basis of the semi-analytic solution of the dynamic equations of motion, the HT of the dynamic response signals has been derived in closed-form. In this way, the resulting analytic signals and their instantaneous amplitudes can be evaluated analytically with limited computational costs.
- The use of reduced Hilbert integrals through suitable integration windows has been proposed to minimize the computational burden involved in the complete HT over the entire time-domain. Additionally, an infinite extension simplification of the free vibrations of high-frequency vibration modes has been also proposed.
- The reported results have shown that integration windows accounting for the interaction of consecutive train axles allow to estimate instantaneous envelopes with minimal jump discontinuities related to truncation errors. In particular, the consideration of integration windows larger than the average axle separation has been shown to be efficient in all the studied cases. Thereby this window length is recommended as an initial tentative value for general application.

- The presented validation case studies have proved the effectiveness of the proposed HTSA model for moderate- and low-damped bridge structures. Nevertheless, the greater presence of fast oscillating components in the dynamic response of low-damped bridges has been shown to increase the sensitivity of the HTSA model to variations in the sampling frequency.

Acknowledgement

The authors wish to express their gratitude to Dr. Pedro Museros (Department of Continuum Mechanics and Theory of Structures, Polytechnic University of Valencia) for his contributions in the original development, ideas, and code used to solve the forward problem by the semi-analytic solution, and also to Mr. Alejandro Castillo-Linares (CEO of ACL-Estructuras) providing real data of the viaducts of Rodenillo and Santa Ana.

This work is part of the project TEP-5066, "Monitorización Estructural predictiva en puentes ferroviarios de alta velocidad", Junta de Andalucía (Spain). The financial support is gratefully acknowledged.

References

[1] E. C. E. Commission, WHITE PAPER roadmap to a single European transport area towards a competitive and resource efficient transport system, COM (2011) 144 (2011).

[2] N. Mazzino, X. Perez, U. Meuser, R. Santoro, M. Brennan, J. Schlaht, C. Chéron, H. Samson, L. Dauby, N. Furio, et al., Rail 2050 Vision: Rail-the Backbone of Europe's Mobility, ERRAC-The European Rail Research Advisory Council, Technical Report (2017).

[3] L. Mao, Y. Lu, Critical speed and resonance criteria of railway bridge response to moving trains, Journal of Bridge Engineering 18 (2011) 131–141.

[4] G. Gu, Resonance in long-span railway bridges carrying TGV trains, Computers & Structures 152 (2015) 185–199.

[5] European Committee for Standardization (CEN), Eurocode 1: Actions on structures - part 2: Traffic loads on bridges, EN 1991-2 Eurocode 1 (2003).

[6] U. I. C. Code, 776-2. design requirements for rail-bridges based on interaction phenomena between train, track and bridge, International Union of Railways (2009).

[7] S. Schneider, S. Marx, Design of railway bridges for dynamic loads due to high-speed traffic, Engineering Structures 174 (2018) 396–406.

[8] J. M. Goicolea, J. Dominguez, J. A. Navarro, F. Gabaldon, New dynamic analysis methods for railway bridges in codes IAPF and Eurocode 1, Railway Bridges Design, Construction and Maintenance, Madrid (2002) 1–43.

[9] M. Zacher, M. Baeßler, Dynamic behaviour of ballast on railway bridges, in: Dynamics of High–Speed Railway Bridges. Selected and revised papers from the Advanced Course on 'Dynamics of High–Speed Railway Bridges', Porto, Portugal, 20–23 September 2005, CRC Press, 2008.

[10] Commitee ERRI D-214.2. Utilisation de convois universels pour le dimensionement dynamique de ponts-rails. Synthèse des résultats du D214.2: Rapport final., 2002.

[11] H. Ouyang, Moving-load dynamic problems: A tutorial (with a brief overview), Mechanical Systems and Signal Processing 25 (2011) 2039 – 2060.

[12] K. Liu, E. Reynders, G. De Roeck, G. Lombaert, Experimental and numerical analysis of a composite bridge for high-speed trains, Journal of Sound and Vibration 320 (2009) 201–220.

[13] M. D. Martínez-Rodrigo, P. Galvín, A. Doménech, A. Romero, Effect of soil properties on the dynamic response of simply-supported bridges under railway traffic through coupled boundary element-finite element analyses, Engineering Structures 170 (2018) 78–90.

[14] A. González, O. Mohammed, Damage detection in bridges based on patterns of dynamic amplification, Structural Control and Health Monitoring 26 (2019) e2361.

[15] Q. Liu, D. J. Thompson, P. Xu, Q. Feng, X. Li, Investigation of train-induced vibration and noise from a steel-concrete composite railway bridge using a hybrid finite element-statistical energy analysis method, Journal of Sound and Vibration (2020) 115197.

[16] B. Noori, R. Arcos, A. Clot, J. Romeu, Control of ground-borne underground railway-induced vibration from double-deck tunnel infrastructures by means of dynamic vibration absorbers, Journal of Sound and Vibration 461 (2019) 114914.

[17] L. Frỳba, Dynamics of railway bridges, Thomas Telford Publishing, 1996.

[18] D. Cantero, T. Arvidsson, E. OBrien, R. Karoumi, Train-track-bridge modelling and review of parameters, Structure and Infrastructure Engineering 12 (2016) 1051–1064.

[19] M. Majka, M. Hartnett, Dynamic response of bridges to moving trains: A study on effects of random track irregularities and bridge skewness, Computers & Structures 87 (2009) 1233–1252.

[20] L. Frỳba, Vibration of solids and structures under moving loads. 3rd ed., Thomas Telford, 1999.

[21] A. Martínez-Castro, P. Museros, A.Castillo-Linares, Semi-analytic solution in the time domain for non-uniform multi-span Bernoulli-Euler beams traversed by moving loads, Journal of Sound and Vibration 294 (2006) 278–297.

[22] A. Martínez-Castro, E. García-Macías, Train-speed sensitivity approach for maximum response envelopes in dynamics of railway bridges, Journal of Sound and Vibration 452 (2019) 13–33.

[23] H. Luo, X. Fang, B. Ertas, Hilbert transform and its engineering applications, AIAA journal 47 (2009) 923–932.

[24] E. C. Titchmarsh, Introduction to the theory of Fourier integrals, Clarendon Press, 1948.

[25] M. Feldman, Hilbert transform in vibration analysis, Mechanical Systems and Signal Processing 25 (2010) (735–802).

[26] M. Simon, G. R. Tomlinson, Use of the Hilbert transform in modal analysis of linear and non-linear structures, Journal of Sound and Vibration 4 (1984) 421–436.

[27] G. R. Tomlinson, Developments in the use of the Hilbert transform for detecting and quantifying non-linearity associated with frequency response functions., Mechanical Systems and Signal Processing 2 (1987) 151–171.

[28] M. Feldman, Non-linear system vibration analysis using Hilbert transform–I. Free vibration analysis method 'Freevib', Mechanical Systems and Signal Processing 2 (1994) 119–127.

[29] M. Feldman, Non-linear system vibration analysis using Hilbert transform–II. Forced vibration analysis method 'Forcevib', Mechanical Systems and Signal Processing 8 (1994) 309–318.

[30] M. Feldman, Hilbert transform applications in mechanical vibration, John Wiley & Sons, 2011.

[31] F. Brancaleoni, D. Spina, C. Valente, Damage assessment from the dynamic response of deteriorating structures, in: Safety Evaluation Based on Identification Approaches Related to Time-Variant and Nonlinear Structures, Springer, 1993, pp. 276–291.

[32] N. E. Huang, S. R. Long, Z. Shen, The mechanism for frequency downshift in nonlinear wave evolution, Advances in Applied Mechanics 32 (1996) 59–117.

[33] N. E. Huang, Z. Shen, S. R. Long, M. C. Wu, H. H. Shih, Q. Zheng, N. C. Yen, C. C. Tung, H. H. Liu, The empirical mode decomposition and the Hilbert spectrum for nonlinear and non-stationary time series analysis, Proceedings of the Royal Society of London. Series A: Mathematical, Physical and Engineering Sciences 454 (1998) 903–995.

[34] N. E. Huang, Z. Shen, S. R. Long, A new view of nonlinear water waves: the Hilbert spectrum, Annual review of fluid mechanics 31 (1999) 417–457.

[35] Z. Y. Shi, S. S. Law, Identification of linear time-varying dynamical systems using Hilbert transform and empirical mode decomposition method, Journal of Applied Mechanics 74 (2007) 223–230.

[36] F. Lo Iacono, G. Navarra, A. Pirrotta, A damage identification procedure based on Hilbert transform: experimental validation, Structural Control and Health Monitoring 19 (2012) 146–160.

[37] Z. Wang, G. Chen, Recursive Hilbert-Huang transform method for time-varying property identification of linear shear-type buildings under base excitations, Journal of Engineering Mechanics 138 (2011) 631–639.

[38] J. N. Yang, Y. Lei, S. Pan, N. Huang, System identification of linear structures based on Hilbert–Huang spectral analysis. Part 1: normal modes, Earthquake engineering & structural dynamics 32 (2003) 1443–1467.

[39] J. N. Yang, Y. Lei, S. Pan, N. Huang, System identification of linear structures based on Hilbert–Huang spectral analysis. Part 2: Complex modes, Earthquake engineering & structural dynamics 32 (2003) 1533–1554.

[40] J. N. Yang, Y. Lei, S. Lin, N. Huang, Identification of natural frequencies and dampings of in situ tall buildings using ambient wind vibration data, Journal of Engineering Mechanics 130 (2004) 570–577.

[41] Z. C. Wang, W. X. Ren, G. D. Chen, A Hilbert transform method for parameter identification of time-varying structures with observer techniques, Smart Materials and Structures 21 (2012) 105007.

[42] B. Chen, S. l. Zhao, P. Y. Li, Application of Hilbert-Huang transform in structural health monitoring: a state-of-the-art review, Mathematical Problems in Engineering 2014 (2014).

[43] P. Museros, A. Martínez-Castro, A. Castillo-Linares, Semi-analytic solution for Kirchhoff plates traversed by moving loads, in: Proceedings of the 6th International Conference on Structural Dynamics. EURODIN 2005, Paris, France, pp. 1619–1624.

[44] A. Martínez-Castro, E. García-Macías, Two techniques for fast evaluation of design envelopes in high-speed train railway bridges: Train speed sensitivity and the Hilbert Transform., in: Proceedings of the 9th International Conference on Structural Dynamics. EURODYN 2014, Porto, Portugal, pp. 1309–1314.

[45] S. L. Hahn, Hilbert transforms in signal processing, Artech House, 1996.

[46] N. E. Huang, N. O. Attoh-Okine, The Hilbert-Huang transform in engineering, CRC Press, 2005.

[47] F. W. King, Hilbert Transforms: Volume 1, Cambridge University Press, 2009.

[48] P. J. Schreier, L. L. Scharf, Statistical signal processing of complex-valued data: the theory of improper and noncircular signals, Cambridge University Press, 2010.

[49] A. H. Nuttall, E. Bedrosian, On the quadrature approximation to the Hilbert transform of modulated signals, Proceedings of the IEEE 54 (1966) 1458–1459.

[50] P. J. Davis, P. Rabinowitz, Methods of numerical integration, Courier Corporation, 2007.

[51] M. Abramowitz, I. A. Stegun, Handbook of mathematical functions: with formulas, graphs, and mathematical tables, volume 55, Courier Corporation, 1965.

[52] Instrucción de acciones a considerar en puentes de ferrocarril (IAPF) [Instruction on actions to be considered in the Project of railway bridges], Standard, Ministerio de Fomento (Spain), 2007.

[53] A. C. Linares, M. V. Fernández, G. M. Poyatos, M. G. Ramírez, J. d. D. M. Jiménez, A. M. Castro, Puente arco sobre la línea de alta velocidad Córdoba-Málaga. Condicionantes dinámicos y constructivos para el diseño [Bowstring arch bridge over the Córdoba-Málaga. Dynamic and constructive design conditions], Hormigón y acero (2010) 25–42.